A Mathematical Study of Topological Phases and Edge Modes in Mechanical Systems

by

Ridvan Ozdemir

A dissertation submitted to the Graduate Faculty of
Auburn University
in partial fulfillment of the
requirements for the Degree of
Doctor of Philosophy

Auburn, Alabama
August 8, 2026

Keywords: Spectral theory, edge modes, topological mechanics

Approved by

Junshan Lin, Chair, Professor of Mathematics and Statistics
Wenxian Shen, Professor of Mathematics and Statistics
Selim Sukhtaiev, Assistant Professor of Mathematics and Statistics
Yimin Zhong, Assistant Professor of Mathematics and Statistics
Siyuan Dai, Associate Professor of Mechanical Engineering

Abstract

In this dissertation, we study topological wave propagation and localization in periodic media. Our main objective is to provide a rigorous mathematical theory to understand the topological phases and the edge modes in topological mechanical systems.

In the first part, we study a one-dimensional periodic spring-mass system consisting of masses connected by springs with different spring constants. The band structure and the topological index, Zak phase, of the system are derived. By gluing two such semi-infinite periodic systems with distinct Zak phases, an interface is obtained. The existence of the edge mode with frequency in the common band gap of two semi-infinite systems is proved by using transfer matrices.

In the second part, we study a two-dimensional mechanical spring-mass system on a honeycomb lattice. The dispersion relation is analyzed and the existence of Dirac points when the masses are identical is proved. We investigate the topological properties of the system when the inversion symmetry is broken by studying the valley Chern number. We provide a proof of the existence of edge modes that are localized at the interface of a joint system constructed from two semi-infinite systems with different valley Chern numbers.

In the final part, we study a gyroscopic system obtained by replacing masses in two-dimensional honeycomb lattice with identical gyroscopes. It results in the breaking of time-reversal symmetry and creates nontrivial topological phases characterized by the Chern numbers. We numerically relate the Chern numbers with the sign of a parameter of the system, namely gravitational acceleration. A joint system is created from two semi-infinite systems with opposite sign Chern numbers. Transfer matrices and a formulation of a finite system obtained from a truncated system are developed in order to study the existence of edge modes. Numerical computations on the finite system provide an evidence of existence of edge modes with frequency in the common band gap of the gyroscopic system. The relationship between transfer matrices and the truncated system is also investigated,

leading several open questions concerning the characterization of the edge states.

Artificial Intelligence (AI) Use Disclosure Statement

In the preparation of this dissertation, ChatGPT (OpenAI) and Claude (Anthropic) are used as tools for language editing and formatting assistance. The scientific content and results are solely my own.

Digital Accessibility Disclosure Statement

In the preparation of this dissertation, LaTeX with LuaLaTeX typesetting engine is used to produce a digitally accessible PDF document. Additional accessibility features, including tagged PDF structure, alternative text for figures, document metadata, and navigational elements, are implemented through the LaTeX accessibility packages and tools provided in the thesis template. The author acknowledges full responsibility for the intellectual content of this work and has made a good faith effort to comply with digital accessibility requirements in publishing, wherein the nature of the content does not significantly change in order to do so. Furthermore, all content has been reviewed and revised to meet these requirements prior to final publication.

Acknowledgments

I would like to express my deepest gratitude to my dear wife, Yagmur, for her endless support. She is my shelter and my biggest supporter through the difficult times of my life and my academic journey. I am grateful for all the sacrifices she has made for us. Without her support, I could not have become the person I am today. She deserves the very best, and I will do my best for her.

I would like to thank my advisor, Dr. Junshan Lin, for his guidance, support, and patience during my PhD studies. I have learned a great deal from him. He has shaped not only my research but also my way of thinking and my approach to teaching. I am proud to have been one of his students.

I am grateful to my parents, Ahmet and Naciye, and my brother, Mehmet. They always support my decisions and do whatever they can for me. My parents' efforts made it possible for me to begin my graduate studies. My brother took care of our parents' needs when I was not there and ensured that my absence was never a burden. I would like to express my gratitude to him.

I would like to thank the members of the committee. The time they devoted to me and the guidance they provided helped me complete my studies.

I would like to thank my previous advisor, Dr. Fatih Ecevit, who supervised me during my master's studies. Beyond his support in my research, he encouraged me to continue when I decided to quit and had a profound impact on my life.

I would like to sincerely thank my friends, Turgay, Ozan, Melike, Keziban, Busra, Furkan, and Dogancan. Their friendship made our time in Auburn enjoyable. Many of my wonderful memories of Auburn are the result of their friendship. Their friendship is one of the greatest gifts Auburn has given me. I wish them all the very best.

Finally, I would like to thank my soccer community in Auburn. I spent countless wonderful hours with them on the field, chasing a soccer ball. They will always be one of the most cherished parts of my time in Auburn and will always hold a special place in my heart. In particular, Gonzalo and my teammates on Independiente USA helped me create unforgettable memories.

This work was partially supported by the NSF grant DMS-2011148.

Table of Contents

List of Figures

Chapter 1

Introduction

1.1 Topological Phase of Matter

The theories on the phases of matter date back to the 1930s with Landau's theory of phase transitions, where materials with the same symmetry were generally considered to be in the same phase [1]. The density difference between solids and liquids is an example of this idea.

The experimental discovery of the integer quantum Hall effect (QHE) in 1980 changed this point of view. An experimental study showed that, under a strong magnetic field, the Hall conductance of a system is quantized in integer multiples of a constant. This quantization is very precise and is not affected by impurities or small changes in the material [2]. This robustness revealed that QHE cannot be explained only by the symmetry argument. Two years later, the theoretical study of the QHE was published [3]. David J. Thouless et al. presented an integer-valued topological invariant associated with the electronic band which determines the quantized Hall conductance, later known as the Chern number. This invariant depends only on the global properties of the Bloch wave functions over the Brillouin zone and is constant under continuous perturbations that do not close the energy gap. The idea that some physical properties depend on topological invariants instead of local material properties was introduced in their study and it became one of the main principles of topological phases. The geometric foundation of Chern number was presented in 1984. Berry introduced the Berry phase and the Berry curvature whose integral over the Brillouin zone gives the Chern number [4].

Several studies on topological phases established a new class of quantum materials, namely topological insulators [5–8]. A topological insulator is a material whose bulk behaves as an insulator due to the energy gap, but its boundary or interface supports conducting states. The interface may appear between a topological insulator and a topologically trivial material or between two topological insulators with different topological indices. Contrary to the classical insulators whose phases are mainly determined by their microscopic properties, such as material parameters or chemical properties, topological insulators are characterized by their global topological invariants which are robust against continuous perturbations that do not close the band gap [9].

The quantum Hall effect enables the characterization of electronic phases by topological invariants. However, it requires a strong magnetic field, which breaks time-reversal symmetry. In 1988, Haldane introduced a honeycomb lattice model [10]. Haldane demonstrated that the topological band structure is a property of the Hamiltonian rather than a consequence of an external effect, such as a magnetic field. Although it is a theoretical model that still breaks time-reversal symmetry, Haldane's model has a nonzero Chern number without an external magnetic field.

Charles L. Kane and Eugene J. Mele, in 2005, introduced graphene with spin-orbit coupling that could have a new quantum phase, namely the quantum spin Hall effect (QSHE), which is distinct from QHE and characterized by another topological invariant they introduced, Z_2. Their idea neither breaks time-reversal symmetry nor needs a magnetic field [5, 6]. In 2007, an experimental study showed the relationship between QSHE and the existence of edge modes and it became the first experimental result of two-dimensional topological insulators [8] which had been predicted by Bernevig et al. [7]. The generalization of Z_2 topological insulators to three dimensions was established by Moore and Balents [11]. For comprehensive reviews, we refer to [12, 13].

1.2 Topological Phases in Periodic Wave Media

The properties of topological edge states, such as their immunity to disorder or defects and the dependence on global properties rather than the tuning of parameters, directed researchers to search for their analogues in classical mechanical systems. Their experimental accessibility and implementability as a counterpart of electronic settings made photonics, acoustics and mechanical structures the major extension areas of topological concepts.

Topological Photonic Materials

Haldane and Raghu proposed the extension of the topological phases to periodic electromagnetic media [14]. They revealed a photonic analog of Chern insulators in two-dimensional photonic crystals by breaking time-reversal symmetry and obtaining edge modes without backscattering. One year later, an experimental result was presented by Wang et al. [15] in which they observed electromagnetic edge states propagating around sharp corners and metallic obstacles. In 2013, time reversal photonic systems were proposed as an analog of QSHE [16]. A systematic analysis of topological photonics which has both theoretical and experimental parts is provided by Lu et al. and Ozawa [17, 18].

Topological Acoustic Materials

Topological acoustic insulators were proposed as an analog of QSHE in 2015 [19]. It is based on circulating fluid flow that breaks time-reversal symmetry and provides acoustic edge modes. This work opened a wide field where many topological acoustic systems were offered, making them attractive for applications due to their formability and flexibility [20–22].

Topological Mechanical Materials

In 2014, the study of topological phenomena was extended to mechanical systems, where the relationship between topological invariants and mechanical boundary modes was studied. Kane and Lubensky analyzed a topological polarization invariant which governs zero-energy surface modes [23]. Chen et al. studied a chain-like linkage that behaves as a topological mechanical insulator and examined edge modes [24].

By constructing a gyroscopic system, Nash et al. provided the first experimental result of a topological mechanical insulator as an analog of the Chern insulators and demonstrated topologically protected chiral mechanical edge modes [25]. The gyroscopic effect causes the breaking of time-reversal symmetry, opens a band gap and creates edge modes that propagate at the boundary of the system and are robust against defects. In the same year, the phononic helical edge states were shown in a macroscopic mechanical system and Z_2 topological mechanical phases were established [26].

The robustness of edge states against defects and disorders makes topological materials attractive for applications. Thus, topological concepts have been studied in various areas where wave propagation is important in the presence of imperfections.

In electronics, the edge states on the surface of a three-dimensional topological insulator enable the creation of metallic conducting channels. They are protected against backscattering due to time-reversal symmetry. In 2008, Fu and Kane showed the existence of edge modes at the interface between a topological insulator and a superconductor which has applications in quantum computing architectures [27, 28]. The robustness of edge modes against imperfections or fabrication errors enables wave guiding in photonic integrated circuits. Topological lasers and valley-selective routing of light are some applications of topological photonics [29, 30]. Vibration isolators and acoustic waveguides are some applications of topological materials in acoustics [31, 32]. Their insensitivity to manufacturing errors and structural damage makes them superior to classical phononic devices.

1.3 Relevant Mathematical Studies

The discovery of topological insulators motivated mathematical research to provide proper mathematical foundations for topological wave phenomena. While the early developments were based on physical intuition and numerical results, mathematical studies aimed to establish rigorous results based on mathematical tools, such as Floquet-Bloch theory, elliptic partial differential equations, spectral theory, and operator theory. These studies created the mathematical descriptions of Dirac points, edge states, interface modes, topological invariants and the bulk-edge correspondence for both discrete and continuous media.

A rigorous theory of Dirac points for two-dimensional Schrödinger operators with honeycomb lattice potentials is presented by Fefferman and Weinstein [33]. Dirac points are the points where bands touch each other in the spectrum of a periodic Hamiltonian with a conical linear dispersion relation (a mathematical definition is given in the following chapters). In their study, they provided a Floquet-Bloch analysis of the Schrödinger operators with the above properties. They showed, under a suitable symmetry, the existence of a conical intersection between two Bloch bands, the linearity of the local dispersion relation near these points and the persistence of Dirac points under a class of perturbations that preserves the relevant symmetry. Dirac points are not just about the linear touching of the bands. When a symmetry is broken, the band gap opens at these points and the system obtains nontrivial topological invariants. For example, the broken inversion symmetry causes the valley Chern numbers of opposite signs and topologically protected edge modes. This rigorous study on Dirac points gave rise to many succeeding studies of topological wave propagation [34–37].

For continuous Schrödinger operators, the foundational works are given by Fefferman, Lee-Thorp, and Weinstein [35, 36]. They showed the bifurcation of edge states with their exponential localization and computed the dispersion curves in the band gap. They also put a distinction between edge states and localized modes. They showed that edge states associated with Dirac points are robust against localized perturbations whereas localized modes are sensitive to small changes and may disappear in the medium. This result provided a characterization of edge states and the effect of Dirac points on edge states. Later, Drouot created a theoretical framework for edge states in general perturbed periodic systems [38]. The study of edge states was extended to a broad class of elliptic operators with honeycomb symmetry by Lee-Thorp, Weinstein, and Zhu [37]. They created an analytic framework for Dirac points and edge states including some applications to graphene and other wave systems. This study showed that the underlying mathematical mechanism of topological edge states is independent of the governing equations of the system.

The study of edge modes in photonic crystals is another research area. Photonic crystals are systems where Maxwell-type operators govern the propagation of electromagnetic waves. Since their structure is similar to those where topological systems are studied, the mathematical tools used in them can be adapted to photonic crystals. An important contribution is on one-dimensional topological photonic materials. Lin and Zhang studied periodic photonic structures with time-reversal symmetry [39]. They predicted the conditions that open a spectral gap around a Dirac point and showed the existence of edge modes in the gap. Qiu et al. studied waveguides bifurcating from Dirac points and provided the conditions of the existence of localized edge modes generated by perturbations of periodic photonic structures [40]. Their study both strengthened the connection among Dirac points, topological invariants and wave localization in photonic crystals and extended the theory to a general class of periodic electromagnetic media.

Another important study is on the valley Hall effect. Chern numbers characterize the topological phases in a system with broken time-reversal symmetry. On the other hand, the valley Hall systems preserve time-reversal symmetry and create the topological behavior from band structures near different Dirac points. Thus, an analysis of them needs a study of the spectral properties near Dirac points [41, 42].

Bulk-edge correspondence is one of the main objectives in topological wave systems.

It states that the number of edge modes at the interface of two topological systems is equal to the difference between their topological invariants. In QHE, the equality of the number of edge states and the Chern number was first studied by Hatsugai [43]. Schulz-Baldes et al. proved that the edge Hall conductivity equals the bulk Hall conductivity by using Kubo-Chern formula and K-theory [44]. In [45], Elbau and Graf provided an alternative operator-theoretic proof for the correspondence based on the index of a pair of projections and extended the result to more general operators. Following this result, Elgart et al. extended the result to systems with a mobility gap. They proved that the equality of the edge Hall conductivity and the bulk edge conductivity is valid even if there is disorder in the system [46]. Bal provided a relationship between the topological invariant and edge modes for continuous models, which is one of the most complete mathematical formulations of bulk-edge correspondence available [47]. Together with two other works on the stability of edge states and a description of topological insulators, Bal showed the effect of the topological invariant on the existence of edge modes in continuous periodic media [48, 49].

1.4 Our Contribution

There are mainly two strategies to realize topological wave insulators using classical waves. The first strategy mimics QHE using active components to break time-reversal symmetry. This is realized by modulating rotational motion of air in acoustic media, applying an external magnetic field in electromagnetic media, or using gyroscopic components in mechanical structures [15, 25, 50]. The second strategy relies on an analog of the quantum spin Hall effect or the quantum valley Hall effect, and it uses passive components to break the inversion symmetry of the system [51–54]. In this dissertation, we study topological phases and edge modes for topological mechanical systems that break either time-reversal symmetry or spatial inversion symmetry. We develop both mathematical theory and computational tools to investigate the underlying mathematical models. Our aim is to provide both rigorous mathematical theory and numerical studies for topological phases and edge modes in mechanical topological systems.

In Chapter 2, we first study a one-dimensional periodic spring-mass system. The setup of the system was introduced in [55]. By using Floquet-Bloch analysis, we determine the band structure of the system. By using the Zak phase as the topological index, we characterize the topological phase of the system and show its value is quantized according to the spring constant, taking the values 0 and π. To analyze the localized edge modes, we create a joint system by gluing two semi-infinite systems with distinct Zak phases. By using the transfer matrix approach, we provide a proof of the existence of an edge mode at the interface of the joint system.

In Chapter 3, we study a two-dimensional spring-mass system over a honeycomb lattice. We first analyze the band structure of the system and show the existence of a band gap. Then we provide a rigorous proof of the existence of Dirac points. To study the bulk properties, we use the valley Chern number to identify the topological phase of the system and prove how it changes according to a structural parameter. We lastly study the existence of edge modes at the interface of a joint system of two systems with opposite-sign valley Chern numbers. We prove the existence of the edge modes by providing wave frequencies in the spectral gap of the system.

In Chapter 4, we study a spring-gyroscope system over a honeycomb lattice. The setup of the system was introduced in [56]. The existence of gyroscopes breaks time-reversal symmetry and results in nontrivial Chern numbers. Firstly, the governing equations of the system are derived. Then we provide a numerical study of the band structure and Chern numbers of the system. A relationship between the Chern number and a parameter of the system is emphasized and a joint system with opposite-sign Chern numbers is constructed to study edge modes. Transfer matrices for the system are constructed. Then, by imposing a boundary condition that depends on the localization of the edge modes, a truncated system is built. Some numerical results on this truncated system are presented and the relationship between the truncated system and the transfer matrix approach is examined, leading to several open mathematical questions concerning the existence of edge modes in spring-gyroscope systems.

Chapter 2

One-dimensional Topological Mechanical Systems

2.1 Periodic Mechanical System

We consider the one-dimensional periodic mechanical system shown in Figure A.1, wherein an infinite array of masses is arranged along the real line. The spring connecting two masses in the unit cell j and two masses between the cell j and $j+1$ attains the spring constants

$$k_1 = k(1+\gamma) \text{ and } k_2 = k(1-\gamma), \tag{2.1}$$

where $\gamma \in (-1, 1)$ is a stiffness parameter and k is the mean stiffness of the springs. The displacements of masses in the unit cell j satisfies the following equations:

$$\begin{aligned} mU''_{a,j} + k_1\left(U_{a,j} - U_{b,j}\right) + k_2\left(U_{a,j} - U_{b,j-1}\right) &= 0, \\ mU''_{b,j} + k_2\left(U_{b,j} - U_{a,j+1}\right) + k_1\left(U_{b,j} - U_{a,j}\right) &= 0. \end{aligned}$$

We consider the solution in the form of

$$U_{a,j}(t) = u_a e^{i(\omega\tau+\mu j)} \text{ and } U_{b,j}(t) = u_b e^{i(\omega\tau+\mu j)} \tag{2.2}$$

where u_a and u_b are the amplitudes of the displacements of masses, j denotes the cell index, ω is the frequency, $\tau = \sqrt{k/m}t$ is a nondimensional time scale and $\mu \in [-\pi, \pi]$ is the nondimensional wave number. Then u_a and u_b satisfy

$$
\begin{aligned}
-m\frac{k}{m}\omega^2 u_a e^{i(\omega\tau+\mu j)} + k(1+\gamma)(u_a - u_b)e^{i(\omega\tau+\mu j)} + k(1-\gamma)(u_a - u_b e^{-i\mu})e^{i(\omega\tau+\mu j)} = 0,\\
-m\frac{k}{m}\omega^2 u_b e^{i(\omega\tau+\mu j)} + k(1+\gamma)(u_b - u_a e^{i\mu})e^{i(\omega\tau+\mu j)} + k(1-\gamma)(u_b - u_a)e^{e^{i(\omega\tau+\mu j)}} = 0.
\end{aligned}
$$

It can be simplified as

$$
\begin{aligned}
\left(2-\Omega^2\right) u_a - (1+\gamma)u_b - (1-\gamma)e^{-i\mu}u_b = 0,\\
\left(2-\Omega^2\right) u_b - (1+\gamma)e^{i\mu}u_a - (1-\gamma)u_a = 0,
\end{aligned}
$$

which reduces to the eigenvalue problem

$$
\begin{bmatrix} 2 & \bar{a}(\mu) \\ a(\mu) & 2 \end{bmatrix} \begin{bmatrix} u_a \\ u_b \end{bmatrix} = \omega^2 \begin{bmatrix} u_a \\ u_b \end{bmatrix}, \tag{2.3}
$$

where $a(\mu) = -(1+\gamma) - (1-\gamma)\, e^{i\mu}$ and $\bar{a}(\mu)$ is the complex conjugate of $a(\mu)$. The characteristic equation of the matrix in (2.3) is

$$
\lambda^2 - 4\lambda + 4 - |a(\mu)|^2 = 0
$$

which gives the eigenpairs

$$
\lambda_{\pm}(\mu) = 2 \pm |a(\mu)| \text{ and } \mathbf{v}_{\pm}(\mu) = \frac{1}{\sqrt{2}} \begin{bmatrix} \frac{\bar{a}(\mu)}{\pm|a(\mu)|} \\ 1 \end{bmatrix},
$$

with $||\mathbf{v}_{\pm}(\mu)||_2 = 1$. We note that if $\gamma \neq 0$, then $|a(\mu)| \neq 0$ and there is a gap between two bands $\lambda_-(\mu)$ and $\lambda_+(\mu)$ for $\mu \in [-\pi, \pi]$. We call this gap the band gap interval

$$
I(\gamma) := (\sqrt{2(1-|\gamma|)}, \sqrt{2(1+|\gamma|)}), \tag{2.4}
$$

where $\sqrt{2(1-|\gamma|)}$ and $\sqrt{2(1+|\gamma|)}$ are the maximum and minimum values of $\sqrt{\lambda_-(\mu)}$ and $\sqrt{\lambda_+(\mu)}$ respectively. We investigate the dynamics of the system for the frequency ω located in the band gap $I(\gamma)$ which is induced by a topological index called the Zak phase.

The Zak phase associated with the frequency band $\lambda(\mu)$ is defined by (cf. [57])

$$\theta^{Zak} = \int_{-\pi}^{\pi} \left[i\left(\mathbf{v}(\mu)\right)^H \partial_\mu \mathbf{v}(\mu)\right] d\mu = -Im\left(\int_{-\pi}^{\pi} \left[\left(\mathbf{v}(\mu)\right)^H \partial_\mu \mathbf{v}(\mu)\right] d\mu\right), \tag{2.5}$$

where $\mathbf{v} = \mathbf{v}_+$ or $\mathbf{v} = \mathbf{v}_-$ is the eigenvector associated with the eigenvalue $\lambda_\pm(\mu)$ of the matrix defined in (2.3) and $\mathbf{v}^H$ stands for the complex conjugate transpose of $\mathbf{v}$. To avoid the difficulties in the calculation of the composition of differentiation and integration, we use the discretization of the integral in (2.5). To this purpose, for $\mu_n = n\pi/N$, $n = -N, -(N-1), ..., N-1, N$ where $N \in \mathbb{Z}^+$, we observe that

$$\begin{aligned}
\log\left[\left(\mathbf{v}(\mu_n)\right)^H \mathbf{v}(\mu_{n+1})\right] &= \log\Big[\left(\mathbf{v}(\mu_n)\right)^H \left(\mathbf{v}(\mu_n) + \partial_\mu \mathbf{v}(\mu_n)(\mu_{n+1}-\mu_n)\right) + O\left(N^{-2}\right)\Big] \\
&= \log\Big[\left(\mathbf{v}(\mu_n)\right)^H \mathbf{v}(\mu_n) + \left(\mathbf{v}(\mu_n)\right)^H \partial_\mu \mathbf{v}(\mu_n)(\mu_{n+1}-\mu_n) \\
&\qquad\qquad + O\left(N^{-2}\right)\Big] \\
&= \log\left[1 + \left(\mathbf{v}(\mu_n)\right)^H \partial_\mu \mathbf{v}(\mu_n)(\mu_{n+1}-\mu_n) + O\left(N^{-2}\right)\right] \\
&= \left(\mathbf{v}(\mu_n)\right)^H \partial_\mu \mathbf{v}(\mu_n)(\mu_{n+1}-\mu_n) + O(N^{-2}).
\end{aligned}$$

Then, by the discretization of the integral, the Zak phase can be written as

$$\begin{aligned}
\theta^{Zak} &= -Im\left(\int_{-\pi}^{\pi} \left[\left(\mathbf{v}(\mu)\right)^H \partial_\mu \mathbf{v}(\mu)\right] d\mu\right) \\
&= -Im\left(\lim_{N\to\infty} \sum_{n=-N}^{N-1} \left(\mathbf{v}(\mu_n)\right)^H \partial_\mu \mathbf{v}(\mu_n)(\mu_{n+1}-\mu_n)\right) \\
&= \lim_{N\to\infty} -\sum_{n=-N}^{N-1} Im\left(\log\left[\left(\mathbf{v}(\mu_n)\right)^H \mathbf{v}(\mu_{n+1})\right]\right).
\end{aligned}$$

We define the discrete Zak phase as

$$\theta_N^{Zak} := -\sum_{n=-N}^{N-1} Im\left(\log\left[\left(\mathbf{v}\left(\mu_n\right)\right)^H \mathbf{v}\left(\mu_{n+1}\right)\right]\right).$$

We have the following lemma for a complex number:

Lemma 1. For a complex number $z = re^{i\theta}$ with $\theta \in [-\pi, \pi]$, if $z + 1 = |z + 1|e^{i\beta}$, there holds

$$\begin{cases} \beta < \theta/2, & \text{for } r < 1, \\ \beta = \theta/2, & \text{for } r = 1, \\ \beta > \theta/2, & \text{for } r > 1. \end{cases}$$

Proof. For $z = a + ib$, the half angle formula gives that

$$\tan(\theta/2) = \frac{\sin(\theta)}{1 + \cos(\theta)} = \frac{b/r}{1 + a/r} = \frac{b}{r + a}.$$

Also, since $\tan(\beta) = \frac{b}{1+a}$, the results follow from the fact that tangent is an increasing function on $[-\pi, \pi]$.

□

Lemma 2. For the Zak phase θ^{Zak} associated with the band $\lambda_-(\mu)$ or $\lambda_+(\mu)$ of the system (2.3), we have

$$\begin{cases} \theta^{Zak} = 0, & \text{if } \gamma > 0, \\ \theta^{Zak} = \pi, & \text{if } \gamma < 0. \end{cases}$$

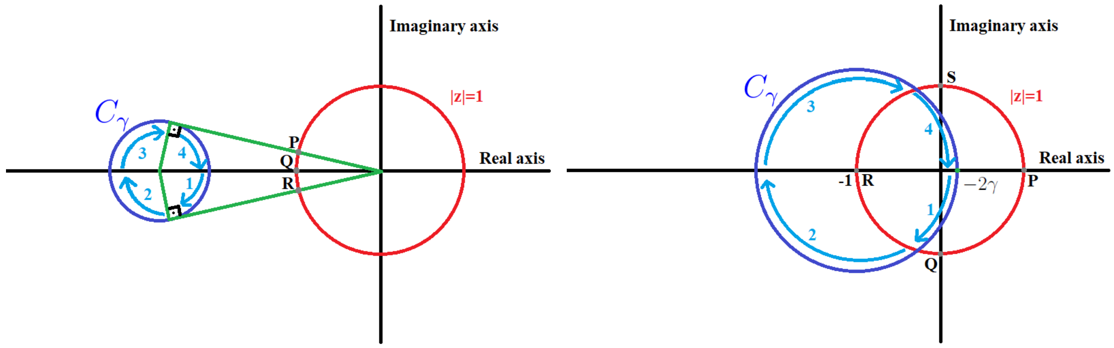

(a) $\gamma > 0$ (b) $\gamma < 0$

Figure 2.1: When $\gamma > 0$, C_γ, the circle with center $-(1+\gamma)$ and radius $1-\gamma$, does not enclose the origin. As $a(\mu)$ completes one turn on C_γ from 1 to 4, the trajectory of $\frac{a(\mu)}{|a(\mu)|}$ is the path $Q \to R \to Q \to P \to Q$ on the unit circle and its argument oscillates near π. When $\gamma < 0$, C_γ contains origin. As $a(\mu)$ completes one turn on C_γ, the trajectory of $\frac{a(\mu)}{|a(\mu)|}$ is the path $P \to Q \to R \to S \to P$ on the unit circle and its argument goes from 2π to 0.

Proof. For $\lambda_+(\mu)$, we have $\mathbf{v} = \mathbf{v}_+$. Let $\theta_n \in [0, 2\pi]$ be the argument of the first component of $\mathbf{v}_+(\mu_n)$. Then a direct computation leads to

$$\begin{aligned}
\mathbf{v}_+^H(\mu_n)\,\mathbf{v}_+(\mu_{n+1}) &= \frac{1}{2}\left(\begin{bmatrix} \frac{a(\mu_n)}{|a(\mu_n)|} & 1 \end{bmatrix} \begin{bmatrix} \frac{\bar{a}(\mu_{n+1})}{|a(\mu_{n+1})|} \\ 1 \end{bmatrix}\right) \\
&= \frac{1}{2}\left(e^{i(\theta_{n+1}-\theta_n)} + 1\right) \\
&= \frac{c_n}{2}\exp\left(i\frac{\theta_{n+1}-\theta_n}{2}\right),
\end{aligned}$$

where c_n is the modulus of $e^{i(\theta_{n+1}-\theta_n)} + 1$ and we have used Lemma 1 in the last step.

Thus the discrete Zak phase

$$
\begin{aligned}
\theta_N^{Zak} &= -\sum_{n=-N}^{N-1} Im\left(\log\left[\mathbf{v}_+^H(\mu_n)\,\mathbf{v}_+(\mu_{n+1})\right]\right) \\
&= -\sum_{n=-N}^{N-1} Im\left(\log\left[\frac{c_n}{2}\left(\exp\left(i\frac{\theta_{n+1}-\theta_n}{2}\right)\right)\right]\right) \\
&= -\sum_{n=-N}^{N-1} Im\left(\log\left(\frac{c_n}{2}\right)+\log\left[\exp\left(i\frac{\theta_{n+1}-\theta_n}{2}\right)\right]\right) \\
&= -\sum_{n=-N}^{N-1} Im\left(\log\left(\frac{c_n}{2}\right)+i\frac{\theta_{n+1}-\theta_n}{2}\right) \\
&= -\sum_{n=-N}^{N-1} \frac{\theta_{n+1}-\theta_n}{2} \\
&= -\frac{\theta_N-\theta_{-N}}{2}.
\end{aligned}
$$

If $\gamma > 0$, we denote the circle with center $-(1+\gamma)$ and radius $1-\gamma$ as C_γ. As μ goes from $-\pi$ to π, $\bar{a}(\mu) = -(1+\gamma)-(1-\gamma)e^{-i\mu}$ completes one turn on the circle C_γ in the clockwise direction starting from the point -2γ on the complex plane. Since $|-(1+\gamma)| = 1+\gamma > 1-\gamma$, the distance between the center of C_γ and the origin is greater than its radius, hence C_γ does not enclose the origin (see Figure 2.1(a)). Therefore, the argument of $\frac{a(\mu)}{|a(\mu)|}$ oscillates around π as μ goes from $-\pi$ to π. As a result, we obtain $\theta_N = \theta_{-N}$ and

$$\theta_N^{Zak} = -\frac{\theta_N-\theta_{-N}}{2} = 0.$$

If $\gamma < 0$, $\bar{a}(\mu)$ still completes one turn on the circle C_γ. However, noting that the distance between the center of C_γ and the origin is less than the radius of C_γ and C_γ encloses the origin. Thus the argument of $\frac{a(\mu)}{|a(\mu)|}$ goes from 2π to 0 (see Figure 2.1(b)) and we have

$$\theta_N^{Zak} = -\frac{\theta_N-\theta_{-N}}{2} = -\frac{0-2\pi}{2} = \pi.$$

For $\lambda_-(\mu)$, we can obtain the same results by similar calculations. Therefore, the proof is complete by noting that $\theta^{Zak} = \lim_{N\to\infty}\theta_N^{Zak}$. $\square$

2.2 Edge Modes for the Topological Mechanical System

We construct a joint system by gluing two periodic mechanical systems with different spring constants as shown in Figure A.2. On the left, the spring constants defined in (2.1) for each unit cell are $k_{1,L} = k(1+\gamma_L)$, $k_{2,L} = k(1-\gamma_L)$ and the spring constants for each unit cell on the right are $k_{1,R} = k(1+\gamma_R)$ and $k_{2,R} = k(1-\gamma_R)$. We assume that γ_L and γ_R have different signs. In light of Lemma 2, these two systems attain different Zak phases, $\theta_L \neq \theta_R$. For $j = 2, 3, ...$, the governing equations for the displacement of the masses at the left and right periodic systems are

$$\begin{aligned} mU''_{a,-j+1} + k_{1,L}\left(U_{a,-j+1} - U_{b,-j+1}\right) + k_{2,L}\left(U_{a,-j+1} - U_{b,-j}\right) = 0, \\ mU''_{b,-j} + k_{2,L}\left(U_{b,-j} - U_{a,-j+1}\right) + k_{1,L}\left(U_{b,-j} - U_{a,-j}\right) = 0, \end{aligned} \tag{2.6}$$

and

$$\begin{aligned} mU''_{a,j} + k_{1,R}\left(U_{a,j} - U_{b,j}\right) + k_{2,R}\left(U_{a,j} - U_{b,j-1}\right) = 0, \\ mU''_{b,j-1} + k_{2,R}\left(U_{b,j-1} - U_{a,j}\right) + k_{1,R}\left(U_{b,j-1} - U_{a,j-1}\right) = 0. \end{aligned} \tag{2.7}$$

respectively. The governing equations for the displacement of the masses located at the interface of the two periodic systems are

$$\begin{aligned} mU''_{a,1} + k_{1,R}\left(U_{a,1} - U_{b,1}\right) + k_{2,L}\left(U_{a,1} - U_{b,-1}\right) = 0, \\ mU''_{b,-1} + k_{2,L}\left(U_{b,-1} - U_{a,1}\right) + k_{1,L}\left(U_{b,-1} - U_{a,-1}\right) = 0. \end{aligned} \tag{2.8}$$

A non-trivial solution $(U_{a,j}(t), U_{b,j}(t))$ for (2.6) - (2.8) which decays to zero as $j \to \pm\infty$ is called an edge mode.

In the rest of this subsection, we aim to show the existence of edge modes for the joint system in Figure A.2 when $\theta_L \neq \theta_R$ and $\omega \in I$, the common band gap, where

$$I := I(\gamma_R) \cap I(\gamma_L) = \left[\sqrt{2(1-|\gamma_R|)}, \sqrt{2(1+|\gamma_R|)}\right] \cap \left[\sqrt{2(1-|\gamma_L|)}, \sqrt{2(1+|\gamma_L|)}\right].$$

Our main result is stated in the following theorem:

Theorem 1. (Existence of edge modes) If $\gamma_L\gamma_R < 0$ such that two periodic mechanical systems with the Zak phase $\theta_L \neq \theta_R$ are glued together as shown in Figure A.2, then there exists an edge mode $(U_{a,j}(t), U_{b,j}(t))$ in the form of

$$U_{a,j}(t) = u_{a,j}e^{i\omega\tau} \text{ and } U_{b,j}(t) = u_{b,j}e^{i\omega\tau} \tag{2.9}$$

for some $\omega \in I$ where j denotes the cell index and τ is the nondimensional time scale.

2.2.1 Transfer Matrix for the Periodic System

Assume that the solutions of (2.6)-(2.7) take the form in (2.9). For the right periodic system, $u_{a,j}$ and $u_{b,j}$ satisfy

$$\begin{aligned}
-m\frac{k}{m}\omega^2 u_{a,j}e^{i\omega\tau} &+ k(1+\gamma_R)\left(u_{a,j}e^{i\omega\tau} - u_{b,j}e^{i\omega\tau}\right)\\
&+ k(1-\gamma_R)\left(u_{a,j}e^{i\omega\tau} - u_{b,j-1}e^{i\omega\tau}\right) = 0,\\
-m\frac{k}{m}\omega^2 u_{b,j-1}e^{i\omega\tau} &+ k(1-\gamma_R)\left(u_{b,j-1}e^{i\omega\tau} - u_{a,j}e^{i\omega\tau}\right)\\
&+ k(1+\gamma_R)\left(u_{b,j-1}e^{i\omega\tau} - u_{a,j-1}e^{i\omega\tau}\right) = 0,
\end{aligned}$$

which implies

$$\begin{aligned}
\left(2-\omega^2\right)u_{a,j} - (1+\gamma_R)u_{b,j} - (1-\gamma_R)u_{b,j-1} &= 0,\\
\left(2-\omega^2\right)u_{b,j-1} - (1-\gamma_R)u_{a,j} - (1+\gamma_R)u_{a,j-1} &= 0.
\end{aligned}$$

This can be written as the system $A\mathbf{u_{j-1}} = B\mathbf{u_j}$, where

$$A = \begin{bmatrix} 0 & 1-\gamma_R \\ -(1+\gamma_R) & 2-\omega^2 \end{bmatrix},\ B = \begin{bmatrix} 2-\omega^2 & -(1+\gamma_R) \\ 1-\gamma_R & 0 \end{bmatrix} \text{ and } \mathbf{u_j} = \begin{bmatrix} u_{a,j} \\ u_{b,j} \end{bmatrix}.$$

We rewrite $A\mathbf{u}_{j-1} = B\mathbf{u}_j$ as

$$T_R \mathbf{u}_{j-1} = \mathbf{u}_j,$$

where the transfer matrix

$$T_R = B^{-1}A = \begin{bmatrix} -\frac{1+\gamma_R}{1-\gamma_R} & \frac{2-\omega^2}{1-\gamma_R} \\ -\frac{2-\omega^2}{1-\gamma_R} & \frac{(2-\omega^2)^2-(1-\gamma_R)^2}{1-\gamma_R^2} \end{bmatrix}.$$

We have

$$\begin{aligned} det(T_R) &= -\frac{1+\gamma_R}{1-\gamma_R}\frac{(2-\omega^2)^2-(1-\gamma_R)^2}{1-\gamma_R^2} - \left(-\frac{2-\omega^2}{1-\gamma_R}\right)\frac{2-\omega^2}{1-\gamma_R} \\ &= -\frac{(2-\omega^2)^2-(1-\gamma_R)^2}{(1-\gamma_R)^2} + \frac{(2-\omega^2)^2}{(1-\gamma_R)^2} \\ &= \frac{(1-\gamma_R)^2}{(1-\gamma_R)^2} \\ &= 1, \end{aligned}$$

with the characteristic equation of T_R

$$\lambda^2 - \left(\frac{(2-\omega^2)^2-(1-\gamma_R)^2-(1+\gamma_R)^2}{1-\gamma_R^2}\right)\lambda + 1 = 0.$$

We observe that

$$\begin{aligned} \left(\frac{(2-\omega^2)^2-(1-\gamma_R)^2-(1+\gamma_R)^2}{1-\gamma_R^2}\right)^2 - 4 &= \frac{\left((2-\omega^2)^2-(1-\gamma_R)^2-(1+\gamma_R)^2\right)^2}{\left(1-\gamma_R^2\right)^2} \\ &\quad - \frac{\left(2(1-\gamma_R^2)\right)^2}{\left(1-\gamma_R^2\right)^2} \\ &= \frac{1}{\left(1-\gamma_R^2\right)^2}\left[\left(2-\omega^2\right)^2-4\right]\left[\left(2-\omega^2\right)^2-4\gamma_R^2\right] \\ &= \frac{1}{\left(1-\gamma_R^2\right)^2}\left[\omega^4-4\omega^2\right]\left[\left(2-\omega^2\right)^2-4\gamma_R^2\right]. \end{aligned}$$

Thus, the eigenvalues of T_R are

$$\lambda_{\pm,R} = \frac{1}{2}\left(\frac{\left(2-\omega^2\right)^2-(1-\gamma_R)^2-(1+\gamma_R)^2}{1-\gamma_R^2}\right.$$
$$\left.\pm\sqrt{\frac{1}{\left(1-\gamma_R^2\right)^2}\left[\omega^4-4\omega^2\right]\left[\left(2-\omega^2\right)^2-4\gamma_R^2\right]}\right)$$
$$= \frac{1}{2(1-\gamma_R^2)}\left(\left(2-\omega^2\right)^2-(1-\gamma_R)^2-(1+\gamma_R)^2\right.$$
$$\left.\pm\sqrt{\omega^2(\omega^2-4)\left[\left(2-\omega^2\right)^2-4\gamma_R^2\right]}\right).$$

The corresponding eigenvectors $\mathbf{e}_{\pm,R}$ are

$$\mathbf{e}_{\pm,R} = \begin{bmatrix} (2-\omega^2) \\ 1+\gamma_R+(1-\gamma_R)\,\lambda_{\pm,R} \end{bmatrix}. \tag{2.10}$$

For the left periodic system, similar calculations give that

$$T_L\mathbf{u}_{-j+1} = \mathbf{u}_{-j}$$

where the transfer matrix

$$T_L = \begin{bmatrix} \frac{(2-\omega^2)^2-(1-\gamma_L)^2}{1-\gamma_L^2} & -\frac{2-\omega^2}{1-\gamma_L} \\ \frac{2-\omega^2}{1-\gamma_L} & \frac{1+\gamma_L}{1-\gamma_L} \end{bmatrix},$$

with eigenvalues

$$\lambda_{\pm,L} := \frac{1}{2(1-\gamma_L^2)}\left(\left(2-\omega^2\right)^2-(1-\gamma_L)^2-(1+\gamma_L)^2\pm\sqrt{\omega^2\left(\omega^2-4\right)\left[\left(2-\omega^2\right)^2-4\gamma_L^2\right]}\right)$$

and the corresponding eigenvector

$$\mathbf{e}_{\pm,L} = \begin{bmatrix} 1+\gamma_L + (1-\gamma_L)\,\lambda_{\pm,L} \\ 2-\omega^2 \end{bmatrix}.$$

Note that we have $\sqrt{2(1-|\gamma_L|)} < \sqrt{2(1+|\gamma_R|)} \le \sqrt{2(1+|\gamma_L|)}$ and $\sqrt{2(1-|\gamma_R|)} < \sqrt{2(1+|\gamma_L|)} \le \sqrt{2(1+|\gamma_R|)}$ when $|\gamma_R| \le |\gamma_L|$ and $|\gamma_L| \le |\gamma_R|$ respectively. It follows that $I \neq \emptyset$.

By taking $\gamma = \min\{|\gamma_R|, |\gamma_L|\}$, $\omega \in I$ gives that

$$\left(\omega^2-2\right)^2 < 2\,(1+\gamma) < 4,$$

thus, $\lambda_{\pm,R}$ and $\lambda_{\pm,L}$ are real. Since $\det(T_R)=1$ and $\lambda_{+,R} \neq \lambda_{-,R}$, one of $|\lambda_{+,R}|$ and $|\lambda_{-,R}|$ is less than 1, $\mathbf{e}_{+,R}$ and $\mathbf{e}_{-,R}$ are linearly independent and $\{\mathbf{e}_{+,R}, \mathbf{e}_{-,L}\}$ form a basis of $\mathbb{R}^2$. Hence, $\mathbf{u}_1 = \begin{bmatrix} u_{a,1} \\ u_{b,1} \end{bmatrix}$ can be written as

$$\mathbf{u}_1 = a_1\mathbf{e}_{+,R} + a_2\mathbf{e}_{-,R}$$

for some constants $a_1, a_2 \in \mathbb{R}$. Then

$$\mathbf{u}_j = T_R^j\mathbf{u}_1 = a_1\left(\lambda_{+,R}\right)^{j-1}\mathbf{e}_{+,R} + a_2\left(\lambda_{-,R}\right)^{j-1}\mathbf{e}_{-,R}.$$

For $\mathbf{u}_j$ to vanish as $j \to \infty$, it is necessary that $\mathbf{u}_1 = \begin{bmatrix} u_{a,1} \\ u_{b,1} \end{bmatrix}$ is parallel to the eigenvector of T_R whose corresponding eigenvalue has absolute value less than 1. Similarly, $\mathbf{u}_{-1} = \begin{bmatrix} u_{a,-1} \\ u_{b,-1} \end{bmatrix}$ must be parallel to the eigenvector of T_L whose corresponding eigenvalue has absolute value less than 1 in order for $\mathbf{u}_j$ to vanish as $j \to -\infty$.

To find the eigenvalues of T_R and T_L with absolute value less than 1, we have

$$
\begin{aligned}
\left(2-\omega^2\right)^2-(1-\gamma_R)^2-(1+\gamma_R)^2 &\leq \left(2\min\{|\gamma_R|\,,|\gamma_L|\}\right)^2-(1-\gamma_R)^2-(1+\gamma_R)^2 \\
&\leq 4\gamma_R^2-1+2\gamma_R-\gamma_R^2-1-2\gamma_R-\gamma_R^2 \\
&= 2(\gamma_R^2-1)\leq 0.
\end{aligned}
$$

Thus $\lambda_{-,R}<\lambda_{+,R}<0$ and the eigenvalue of T_R with absolute value less than 1 is

$$
\begin{aligned}
\lambda_R := \lambda_{+,R} = \frac{1}{2(1-\gamma_R^2)}\Bigg(&\left(2-\omega^2\right)^2-(1-\gamma_R)^2-(1+\gamma_R)^2 \\
&+\omega\sqrt{(\omega^2-4)\left[\left(2-\omega^2\right)^2-4\gamma_R^2\right]}\Bigg).
\end{aligned}
$$

The corresponding eigenvector $\mathbf{e}_R$ is

$$
\mathbf{e}_R := \mathbf{e}_{+,R} = \begin{bmatrix} (2-\omega^2) \\ 1+\gamma_R+(1-\gamma_R)\,\lambda_R \end{bmatrix}. \tag{2.11}
$$

By similar calculations, we obtain

$$
\lambda_L := \frac{1}{2(1-\gamma_L^2)}\left(\left(2-\omega^2\right)^2-(1-\gamma_L)^2-(1+\gamma_L)^2+\omega\sqrt{(\omega^2-4)\left[\left(2-\omega^2\right)^2-4\gamma_L^2\right]}\right)
$$

and the corresponding eigenvector

$$
\mathbf{e}_L = \begin{bmatrix} 1+\gamma_L+(1-\gamma_L)\,\lambda_L \\ 2-\omega^2 \end{bmatrix}. \tag{2.12}
$$

Therefore, we obtain that $\mathbf{u}_1=\begin{bmatrix} u_{a,1} \\ u_{b,1}\end{bmatrix}$ must be parallel to $\mathbf{e}_R$ and $\mathbf{u}_{-1}=\begin{bmatrix} u_{a,-1} \\ u_{b,-1}\end{bmatrix}$ must be parallel to $\mathbf{e}_L$ to vanish as $j\to\pm\infty$.

2.2.2 Proof of Theorem 1

By substituting (2.9) into the equations (2.8), we get

$$\begin{aligned} \left(2-\omega^2+\gamma_R-\gamma_L\right)u_{a,1}-\left(1+\gamma_R\right)u_{b,1}-\left(1-\gamma_L\right)u_{b,-1}&=0, \\ \left(2-\omega^2\right)u_{b,-1}-\left(1-\gamma_L\right)u_{a,1}-\left(1+\gamma_L\right)u_{a,-1}&=0. \end{aligned} \tag{2.13}$$

Since $\begin{bmatrix} u_{a,1} \\ u_{b,1} \end{bmatrix}$ and $\begin{bmatrix} u_{a,-1} \\ u_{b,-1} \end{bmatrix}$ are parallel to $\mathbf{e}_R$ and $\mathbf{e}_L$ respectively, there holds

$$\begin{bmatrix} u_{a,1} \\ u_{b,1} \end{bmatrix} = c_1\mathbf{e}_R \text{ and } \begin{bmatrix} u_{a,-1} \\ u_{b,-1} \end{bmatrix} = c_2\mathbf{e}_L$$

for some constants c_1 and c_2. Then by (2.13), we obtain

$$\begin{aligned} &\left(2-\omega^2+\gamma_R-\gamma_L\right)c_1\left(2-\omega^2\right)-\left(1+\gamma_R\right)c_1\left(1+\gamma_R+\left(1-\gamma_R\right)\lambda_R\right) \\ &\qquad -\left(1-\gamma_L\right)c_2\left(2-\omega^2\right)=0, \\ &\left(2-\omega^2\right)c_2\left(2-\omega^2\right)-\left(1-\gamma_L\right)c_1\left(2-\omega^2\right) \\ &\qquad -\left(1+\gamma_L\right)c_2\left(1+\gamma_L+\left(1-\gamma_L\right)\lambda_L\right)=0. \end{aligned} \tag{2.14}$$

(2.14) can be simplified as

$$\begin{aligned} \left[\Omega^2+\left(\gamma_R-\gamma_L\right)\Omega-\left(1+\gamma_R\right)^2-\left(1-\gamma_R^2\right)\lambda_R\right]c_1&=\left(1-\gamma_L\right)\Omega c_2, \\ \left[\Omega^2-\left(1+\gamma_L\right)^2-\left(1-\gamma_L^2\right)\lambda_L\right]c_2&=\left(1-\gamma_L\right)\Omega c_1, \end{aligned} \tag{2.15}$$

where $\Omega=2-\omega^2$. Multiplying the second equation in (2.15) by $\left(1-\gamma_L\right)\Omega$ gives

$$\left[\Omega^2-\left(1+\gamma_L\right)^2-\left(1-\gamma_L^2\right)\lambda_L\right]\left(1-\gamma_L\right)\Omega c_2=\left(1-\gamma_L\right)^2\Omega^2c_1. \tag{2.16}$$

By the first equation in (2.15) and (2.16), we have

$$\left[\Omega^2-(1+\gamma_L)^2-(1-\gamma_L^2)\,\lambda_L\right]\left[\Omega^2+(\gamma_R-\gamma_L)\,\Omega-(1+\gamma_R)^2-(1-\gamma_R^2)\,\lambda_R\right]$$
$$=(1-\gamma_L)^2\,\Omega^2,$$

which can be simplified as

$$\left[\Omega^2-4\gamma_L-\sqrt{(4-\Omega^2)\,(4\gamma_L^2-\Omega^2)}\right]\left[\Omega^2+2\,(\gamma_R-\gamma_L)\,\Omega-4\gamma_R-\sqrt{(4-\Omega^2)\,(4\gamma_R^2-\Omega^2)}\right]$$
$$=4\,(1-\gamma_L)^2\,\Omega^2. \tag{2.17}$$

Observe that, for $\Omega=0$, we have

$$\left[0^2-4\gamma_L-\sqrt{(4-0^2)\,(4\gamma_L^2-0^2)}\right]\left[0^2+2\,(\gamma_R-\gamma_L)\,0-4\gamma_R-\sqrt{(4-0^2)\,(4\gamma_R^2-0^2)}\right]$$
$$=4\,(1-\gamma_L)^2\,0^2$$

which is equivalent to

$$(\gamma_L+|\gamma_L|)\,(\gamma_R+|\gamma_R|)=0. \tag{2.18}$$

Since γ_L and γ_R have different signs, either $\gamma_L+|\gamma_L|=0$ or $\gamma_R+|\gamma_R|=0$. Therefore, (2.18) holds and $\Omega=0$ is a solution of (2.17). Note that $\Omega=0$ gives $\omega=\sqrt{2}\in I$. This proves the theorem.

Chapter 3

Two-dimensional Honeycomb Topological Mechanical System

3.1 Periodic Mechanical System

3.1.1 Mathematical Model

We consider the two-dimensional mechanical system over the honeycomb lattice as shown in Figure B.1(a). Let $\mathbf{a}_1 = a[1,0]$ and $\mathbf{a}_2 = a[\frac{1}{2}, \frac{\sqrt{3}}{2}]$ be the lattice vectors where a is the lattice constant. Then the honeycomb lattice is given by $\Lambda := \sum\limits_{p,q\in\mathbb{Z}} Y_{p,q}$, where $Y_{p,q} = \{(p+t_1)\mathbf{a}_1 + (q+t_2)\mathbf{a}_2 : 0 \leq t_1, t_2 \leq 1\}$ as shown in Figure B.1(b). Each periodic cell contains two masses, $m_a = m(1+\beta)$ and $m_b = m(1-\beta)$ with $-1 < \beta < 1$, connected by a spring of length $\frac{a}{\sqrt{3}}$ and the spring constant k. Let $\mathbf{b}_1$ and $\mathbf{b}_2$ be the reciprocal lattice vectors given by $\mathbf{b}_1 = \frac{2\pi}{a}\left[1, -\frac{1}{\sqrt{3}}\right]$ and $\mathbf{b}_2 = \frac{2\pi}{a}\left[0, \frac{2}{\sqrt{3}}\right]$, which satisfy

$$\mathbf{a}_i \cdot \mathbf{b}_j = 2\pi\delta_{ij} = \begin{cases} 0, \ i \neq j, \\ 2\pi, \ i = j. \end{cases}$$

The hexagonal shape of the fundamental cell in the reciprocal lattices $\Lambda^* := \sum_{p,q\in\mathbb{Z}} p\mathbf{b}_1 + q\mathbf{b}_2$, or the Brillouin zone $\mathbb{B}$, is shown in Figure 3.1. Over the periodic cell $Y_{p,q}$, the displacements $U^a_{p,q}(t)$ and $U^b_{p,q}(t)$ for the masses a and b satisfy

$$\begin{aligned} m_a(U^a_{p,q})'' + k\left(3U^a_{p,q} - U^b_{p,q} - U^b_{p-1,q} - U^b_{p,q-1}\right) = 0, \\ m_b(U^b_{p,q})'' + k\left(3U^b_{p,q} - U^a_{p,q} - U^a_{p+1,q} - U^a_{p,q+1}\right) = 0. \end{aligned} \tag{3.1}$$

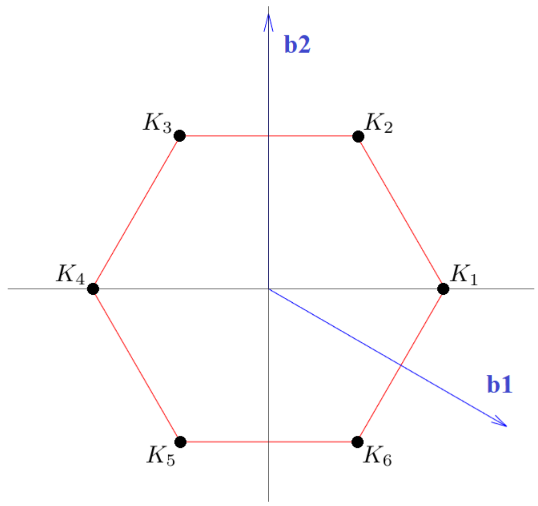

Figure 3.1: The Brillouin zone $\mathbb{B}$ in the reciprocal lattice. The vertices of the Brillouin zone are $K_1 = \left(\frac{4\pi}{3a}, 0\right)$, $K_2 = \left(\frac{2\pi}{3a}, \frac{2\pi}{a\sqrt{3}}\right)$, $K_3 = \left(-\frac{2\pi}{3a}, \frac{2\pi}{a\sqrt{3}}\right)$, $K_4 = \left(-\frac{4\pi}{3a}, 0\right)$, $K_5 = \left(-\frac{2\pi}{3a}, -\frac{2\pi}{a\sqrt{3}}\right)$ and $K_6 = \left(\frac{2\pi}{3a}, -\frac{2\pi}{a\sqrt{3}}\right)$.

Consider the time-harmonic solution in the form of

$$U^a_{p,q}(t) = u_a \exp\left[i(\omega\tau + \boldsymbol{\kappa}\cdot\mathbf{r}_{p,q})\right] \text{ and } U^b_{p,q}(t) = u_b \exp\left[i(\omega\tau + \boldsymbol{\kappa}\cdot\mathbf{r}_{p,q})\right], \tag{3.2}$$

where $\tau = \sqrt{k/m}t$ is nondimensional time scale, u_a and u_b are the amplitudes of displacements, the position vector $\mathbf{r_{p,q}} = p\mathbf{a}_1 + q\mathbf{a}_2$, the wave vector $\boldsymbol{\kappa} = \kappa_1\mathbf{b}_1 + \kappa_2\mathbf{b}_2$, and the wave frequency ω. Then (3.2) becomes

$$m(1+\beta)\frac{k}{m}(-\omega^2)u_a e^{i(\omega\tau+\boldsymbol{\kappa}\cdot\mathbf{r}_{p,q})} + k\left(3u_a - u_b - e^{-i\boldsymbol{\kappa}\cdot\mathbf{a}_1}u_b - e^{-i\boldsymbol{\kappa}\cdot\mathbf{a}_2}u_b\right)e^{i(\omega\tau+\boldsymbol{\kappa}\cdot\mathbf{r}_{p,q})} = 0,$$
$$m(1-\beta)\frac{k}{m}(-\omega^2)u_b e^{i(\omega\tau+\boldsymbol{\kappa}\cdot\mathbf{r}_{p,q})} + k\left(3u_b - u_a - -e^{i\boldsymbol{\kappa}\cdot\mathbf{a}_1}u_a - -e^{i\boldsymbol{\kappa}\cdot\mathbf{a}_2}u_a\right)e^{i(\omega\tau+\boldsymbol{\kappa}\cdot\mathbf{r}_{p,q})} = 0,$$

and u_a and u_b satisfy

$$(1+\beta)(-\omega^2)u_a + 3u_a + (-1 - e^{-i\boldsymbol{\kappa}\cdot\boldsymbol{a}_1} - e^{-i\boldsymbol{\kappa}\cdot\boldsymbol{a}_2})u_b = 0,$$
$$(1-\beta)(-\omega^2)u_b + 3u_b + (-1 - e^{i\boldsymbol{\kappa}\cdot\boldsymbol{a}_1} - e^{i\boldsymbol{\kappa}\cdot\boldsymbol{a}_2})u_a = 0,$$

or equivalently,

$$M(\boldsymbol{\kappa})\, \boldsymbol{v}(\boldsymbol{\kappa}) = \omega^2 \boldsymbol{v}(\boldsymbol{\kappa}), \tag{3.3}$$

wherein

$$M(\boldsymbol{\kappa}) := \begin{bmatrix} \frac{3}{1+\beta} & \frac{\overline{d(\kappa)}}{1+\beta} \\ \frac{d(\kappa)}{1-\beta} & \frac{3}{1-\beta} \end{bmatrix} \text{ and } \boldsymbol{v}(\boldsymbol{\kappa}) := \begin{bmatrix} u_a \\ u_b \end{bmatrix}. \tag{3.4}$$

In the above, $d(\boldsymbol{\kappa}) := -1 - e^{i\boldsymbol{\kappa}\cdot\boldsymbol{a}_1} - e^{i\boldsymbol{\kappa}\cdot\boldsymbol{a}_2} = -1 - e^{i2\pi\kappa_1} - e^{i2\pi\kappa_2}$ and $\overline{d(\boldsymbol{\kappa})}$ is the complex conjugate of $d(\boldsymbol{\kappa})$. We have

$$det(M(\boldsymbol{\kappa})) = \frac{3}{1+\beta}\frac{3}{1-\beta} - \frac{\overline{d(\kappa)}}{1+\beta}\frac{d(\kappa)}{1-\beta} = \frac{9-|d(\boldsymbol{\kappa})|^2}{1-\beta^2},$$

and the characteristic equation is

$$\lambda^2 - \frac{6}{1-\beta^2}\lambda + \frac{9-|d(\boldsymbol{\kappa})|^2}{1-\beta^2} = 0.$$

Thus, the eigenvalues of the matrix $M(\boldsymbol{\kappa})$ are

$$\begin{aligned} \lambda_{\pm}(\boldsymbol{\kappa}) &= \frac{1}{2}\left(\frac{6}{1-\beta^2} \pm \sqrt{\left(\frac{6}{1-\beta^2}\right)^2 - 4\frac{9-|d(\boldsymbol{\kappa})|^2}{1-\beta^2}}\right) \\ &= \frac{3}{1-\beta^2} \pm \sqrt{\frac{9\beta^2}{(1-\beta^2)^2} + \frac{|d(\boldsymbol{\kappa})|^2}{1-\beta^2}}, \end{aligned} \tag{3.5}$$

with the corresponding eigenvectors

$$\boldsymbol{v}_{\pm}(\boldsymbol{\kappa}) = \frac{1}{\chi(\boldsymbol{\kappa})}\begin{bmatrix} -\frac{\overline{d(\boldsymbol{\kappa})}}{3-\lambda_{\pm}(\boldsymbol{\kappa})(1+\beta)} \\ 1 \end{bmatrix}. \tag{3.6}$$

In the above, $\chi(\boldsymbol{\kappa})$ is a normalization constant such that

$$\boldsymbol{v}_{\pm}^{*}(\boldsymbol{\kappa})\begin{bmatrix}1+\beta & 0\\ 0 & 1-\beta\end{bmatrix}\boldsymbol{v}_{\pm}(\boldsymbol{\kappa})=1, \tag{3.7}$$

where $\boldsymbol{v}_{\pm}^{*}(\boldsymbol{\kappa})$ is the conjugate transpose of $\boldsymbol{v}_{\pm}(\boldsymbol{\kappa})$. In what follows, we use d, M, λ and $\boldsymbol{v}$ instead of $d(\boldsymbol{\kappa})$, $M(\boldsymbol{\kappa})$ $\lambda(\boldsymbol{\kappa})$ and $\boldsymbol{v}(\boldsymbol{\kappa})$ for simplicity.

3.1.2 Dirac Point when $\beta = 0$

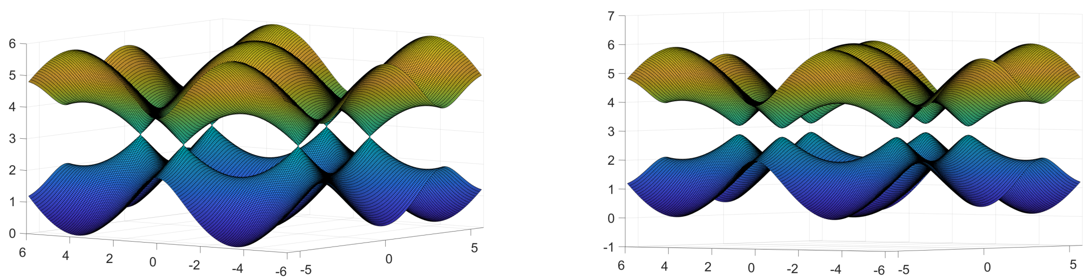

(a) $\beta = 0$ (b) $\beta = 0.05$

Figure 3.2: The band structure of the periodic system. (a) $\beta = 0$: The upper and lower bands touch at the vertices of Brillouin zone and form the Dirac points. (b) $\beta \neq 0$: A gap opens between the two bands.

We first study the band structure when the two masses $m_a = m_b$, namely when $\beta = 0$. In particular, we show that a Dirac point exists at the vertices of the Brillouin zone. A pair $(\boldsymbol{\kappa}^*, \lambda^*) \in \mathbb{B} \times \mathbb{R}$ is called a Dirac point (cf. [58],[37],[59], [34]) if

1. $\lambda_+(\boldsymbol{\kappa}^*) = \lambda_-(\boldsymbol{\kappa}^*) = \lambda^*$. In addition, there exist constants $\alpha > 0$ and $\gamma > 0$ such that the expansions

$$\lambda_+(\boldsymbol{\kappa}) = \lambda^* + \alpha|\boldsymbol{\kappa} - \boldsymbol{\kappa}^*| + O\left(|\boldsymbol{\kappa}|^2\right),$$
$$\lambda_-(\boldsymbol{\kappa}) = \lambda^* - \alpha|\boldsymbol{\kappa} - \boldsymbol{\kappa}^*| + O\left(|\boldsymbol{\kappa}|^2\right),$$

hold for $|\boldsymbol{\kappa} - \boldsymbol{\kappa}^*| < \gamma$.

2. The eigenvalue $\lambda_{\pm}(\boldsymbol{\kappa})$ in (3.5) has multiplicity two when $\boldsymbol{\kappa} = \boldsymbol{\kappa}^*$.

Remark 1. Observe that if $\boldsymbol{\kappa}_i = K_i$, then $\boldsymbol{\kappa}_1 = \boldsymbol{\kappa}_3 + \boldsymbol{b}_1$, $\boldsymbol{\kappa}_3 = \boldsymbol{\kappa}_5 + \boldsymbol{b}_2$, $\boldsymbol{\kappa}_2 = \boldsymbol{\kappa}_6 + \boldsymbol{b}_2$ and $\boldsymbol{\kappa}_6 = \boldsymbol{\kappa}_4 + \boldsymbol{b}_1$. Therefore,

$$\begin{aligned}
d(\boldsymbol{\kappa}_1) = -1 - e^{i\boldsymbol{\kappa}_1\cdot\boldsymbol{a}_1} - e^{i\boldsymbol{\kappa}_1\cdot\boldsymbol{a}_2} &= -1 - e^{i(\boldsymbol{\kappa}_3+\mathbf{b}_1)\cdot\boldsymbol{a}_1} - e^{i(\boldsymbol{\kappa}_3+\mathbf{b}_1)\cdot\boldsymbol{a}_2} \\
&= -1 - e^{i\boldsymbol{\kappa}_3\cdot\boldsymbol{a}_1} e^{i\boldsymbol{b}_1\cdot\boldsymbol{a}_1} - e^{i\boldsymbol{\kappa}_3\cdot\boldsymbol{a}_2} e^{i\boldsymbol{b}_1\cdot\boldsymbol{a}_2} \\
&= -1 - e^{i\boldsymbol{\kappa}_3\cdot\boldsymbol{a}_1} e^{i2\pi} - e^{i\boldsymbol{\kappa}_3\cdot\boldsymbol{a}_2} e^{0} \\
&= -1 - e^{i\boldsymbol{\kappa}_3\cdot\boldsymbol{a}_1} - e^{i\boldsymbol{\kappa}_3\cdot\boldsymbol{a}_2} \\
&= d(\boldsymbol{\kappa}_3).
\end{aligned}$$

By similar calculations, we have

$$d(\boldsymbol{\kappa}_1) = d(\boldsymbol{\kappa}_3) = d(\boldsymbol{\kappa}_5) \ \text{ and } \ d(\boldsymbol{\kappa}_2) = d(\boldsymbol{\kappa}_4) = d(\boldsymbol{\kappa}_6), \tag{3.8}$$

and it is sufficient to study the eigenvalues for $\boldsymbol{\kappa} = K_1$ and $\boldsymbol{\kappa} = K_4$.

When $\beta = 0$, from (3.5), the eigenvalues of M in (3.3) are

$$\lambda(\boldsymbol{\kappa}) = 3 \pm |d(\boldsymbol{\kappa})|.$$

Observe that

$$d(K_1) = -1 - \exp\left(ia\frac{4\pi}{3a}\right) - \exp\left(ia\frac{\frac{4\pi}{3a} + 0\sqrt{3}}{2}\right) = 0.$$

We obtain $\lambda_+(K_1) = \lambda_-(K_1) = 3$ (Figure 3.2(a)). In addition, the derivative of $\lambda_+(\boldsymbol{\kappa})$ at

$\boldsymbol{\kappa} = K_1$ along the direction $\mathbf{w} = (w_1, w_2)$ is

$$
\begin{aligned}
D_{\boldsymbol{w}}\lambda_+ (K_1) &= \lim_{h\to 0^+} \frac{1}{h}\left[\lambda_+\left(\frac{4\pi}{3a} + w_1 h, 0 + w_2 h\right) - \lambda_+\left(\frac{4\pi}{3a}, 0\right)\right] \\
&= \lim_{h\to 0^+} \sqrt{\frac{1}{h^2}\left[4\cos^2\left[\frac{2\pi}{3} + \frac{w_1 a}{2}h\right] + 4\cos\left[\frac{2\pi}{3} + \frac{w_2 a}{2}h\right] + 1\right]} = \frac{a\sqrt{3}}{2}.
\end{aligned}
$$

Similarly,

$$
D_{\boldsymbol{w}}\lambda_- (K_1) = -\frac{a\sqrt{3}}{2}.
$$

Therefore, near K_1, there holds

$$
\lambda_\pm (\boldsymbol{\kappa}) = 3 \pm \frac{a\sqrt{3}}{2}\left|\boldsymbol{\kappa} - K_1\right| + O\left(\left|\boldsymbol{\kappa} - K_1\right|^2\right).
$$

Following similar calculations, it can be shown that, for $\boldsymbol{\kappa}$ near K_4,

$$
\lambda_\pm (\boldsymbol{\kappa}) = 3 \pm \frac{a\sqrt{3}}{2}\left|\boldsymbol{\kappa} - K_4\right| + O\left(\left|\boldsymbol{\kappa} - K_4\right|^2\right).
$$

Note that we have $M(\boldsymbol{\kappa}) = \begin{bmatrix} 3 & 0 \\ 0 & 3 \end{bmatrix}$ for $\boldsymbol{\kappa} = K_1, K_4$. Thus, the multiplicity of λ^* is 2. Therefore, $(K_i, 3)$ is a Dirac point for $i = 1, 4$.

Remark 2. When $\beta \neq 0$, we have $\lambda_- (\boldsymbol{\kappa}) < \lambda_+ (\boldsymbol{\kappa})$ for $\boldsymbol{\kappa} \in \mathbb{B}$ and there is a gap between the upper and lower bands $\lambda_\pm (\boldsymbol{\kappa})$ in (3.6) which is called band gap.

3.1.3 Valley Chern Number

The Berry phase is a phase angle that describes the global phase change of a complex vector over a closed loop ν in its parameter space. The Berry phase associated with the band λ of the system in (3.3) is defined as a line integral around a closed loop ν in the

Brillouin zone (cf. [57]);

$$\phi = \oint_{\nu} \boldsymbol{B}(\boldsymbol{\kappa}) d\boldsymbol{\kappa}. \tag{3.9}$$

In the above, $\boldsymbol{B}(\boldsymbol{\kappa}) = (A_{\kappa_x}(\boldsymbol{\kappa}), A_{\kappa_y}(\boldsymbol{\kappa}))$ is the Berry connection, wherein

$$A_j(\boldsymbol{\kappa}) := \langle \boldsymbol{v}(\boldsymbol{\kappa}), i\partial_j \boldsymbol{v}(\boldsymbol{\kappa}) \rangle, \;\; j = \kappa_x, \kappa_y,$$

and $\boldsymbol{v}$ is the eigenvector of M associated with the eigenvalue λ as defined in (3.6). By Stokes' theorem,

$$\phi = \int_D \Omega(\boldsymbol{\kappa}) dS, \tag{3.10}$$

where D is the region enclosed by ν and $\Omega(\boldsymbol{\kappa})$ is the Berry curvature given by $\Omega(\boldsymbol{\kappa}) = \partial_{\kappa_x} A_{\kappa_y}(\boldsymbol{\kappa}) - \partial_{\kappa_y} A_{\kappa_x}(\boldsymbol{\kappa})$. The valley Chern number for a Bloch wave vector $\boldsymbol{\kappa} = K$ is defined as the Berry phase calculated over a closed loop ν containing K scaled by 2π (cf. [60]), i.e.,

$$C_{K,\nu} = \frac{1}{2\pi}\left(\oint_{\nu} B(\boldsymbol{\kappa}) d\boldsymbol{\kappa} \pmod{2\pi}\right) = \frac{1}{2\pi}\int_D \Omega(\boldsymbol{\kappa}) dS. \tag{3.11}$$

Remark 3. For the eigenvector $\boldsymbol{v}$ of the system in (3.3), a gauge transformation $\tilde{\boldsymbol{v}}(\boldsymbol{\kappa}) = e^{-i\varphi(\boldsymbol{\kappa})}\boldsymbol{v}(\boldsymbol{\kappa})$ for a differentiable phase function $\varphi(\boldsymbol{\kappa})$ gives $\tilde{\boldsymbol{B}}(\boldsymbol{\kappa}) = \boldsymbol{B}(\boldsymbol{\kappa}) + \nabla\varphi(\boldsymbol{\kappa})$. In light of (3.9), the Berry phase $\tilde{\phi} = \phi + 2\pi m$, for some $m \in \mathbb{Z}$, but $\tilde{\Omega}(\boldsymbol{\kappa}) = \Omega(\boldsymbol{\kappa})$ since $\nabla \times \nabla\varphi = 0$ (cf. [57], [61], [62]). As such we use modulo 2π in (3.11) when the Berry connection is used.

Let ν be a circle centered at K with radius $0 < r \ll 1$, we define the discrete valley Chern number as, for $N \in \mathbb{Z}^+$,

$$C_{K,\nu}^N = -\frac{1}{2\pi}\left[Im\left(\sum_{j=1}^{N}\log\langle \boldsymbol{v}\left(K+\boldsymbol{\kappa}_j\right), \boldsymbol{v}\left(K+\boldsymbol{\kappa}_{j+1}\right)\rangle\right) \pmod{2\pi}\right], \tag{3.12}$$

where $\boldsymbol{\kappa}_j = r\left(\cos\left(\theta_j\right), \sin\left(\theta_j\right)\right)$, $\theta_j = -\pi + (j-1)\frac{2\pi}{N}$. It is clear that

$$C_{K,\nu} = \lim_{N\to\infty} C_{K,\nu}^N.$$

In what follows, we use C_K instead of $C_{K,\nu}$ for simplicity.

Lemma 3. For $N = 2n \in \mathbb{Z}^+$

1. The Berry phase ϕ over the Brillouin zone is zero.
2. The valley Chern numbers for the vertices of the Brillouin zone satisfy

   $$C_{K_1}^N = C_{K_3}^N = C_{K_5}^N \text{ and } C_{K_2}^N = C_{K_4}^N = C_{K_6}^N.$$

   In addition, the valley Chern numbers satisfy $C_{K_1}^N = -C_{K_4}^N$.
3. Let $\boldsymbol{v}_\pm$ be the eigenvectors of M defined in (3.6). If $\boldsymbol{v} = \boldsymbol{v}_+$, β and $C_{K_1}^N$ attain opposite signs, and if $\boldsymbol{v} = \boldsymbol{v}_-$, β and $C_{K_1}^N$ attain the same signs, where $\boldsymbol{v}_\pm$ is the vector given in (3.6).

Proof. (i) For $N = 2n$ with $n \in \mathbb{Z}^+$, let $\left\{\hat{\boldsymbol{\kappa}}_j\right\}_{j=1}^N$ be equally spaced points on the boundary of the Brillouin zone. Then, for $j = 1, 2, ..., n+1$, we have

$$\hat{\boldsymbol{\kappa}}_j = -\hat{\boldsymbol{\kappa}}_{n+j},$$

which implies

$$d\left(\hat{\boldsymbol{\kappa}}_{j+n}\right)=-1-e^{i\hat{\boldsymbol{\kappa}}_{j+n}\cdot\boldsymbol{a}_1}-e^{i\hat{\boldsymbol{\kappa}}_{j+n}\cdot\boldsymbol{a}_2}=-1-e^{-i\hat{\boldsymbol{\kappa}}_j\cdot\boldsymbol{a}_1}-e^{-i\hat{\boldsymbol{\kappa}}_j\cdot\boldsymbol{a}_2}=\overline{d\left(\hat{\boldsymbol{\kappa}}_j\right)}$$

and thus

$$\boldsymbol{v}\left(\hat{\boldsymbol{\kappa}}_{j\pm n}\right)=\frac{1}{\chi\left(\hat{\boldsymbol{\kappa}}_{j\pm n}\right)}\begin{bmatrix}-\frac{\overline{d\left(\hat{\boldsymbol{\kappa}}_{j\pm n}\right)}}{3-\lambda_{\pm}\left(\hat{\boldsymbol{\kappa}}_{j\pm n}\right)(1+\beta)}\\ 1\end{bmatrix}=\frac{1}{\overline{\chi\left(\hat{\boldsymbol{\kappa}}_j\right)}}\begin{bmatrix}-\frac{d\left(\hat{\boldsymbol{\kappa}}_j\right)}{3-\lambda_{\pm}\left(\hat{\boldsymbol{\kappa}}_j\right)(1+\beta)}\\ 1\end{bmatrix}=\overline{\boldsymbol{v}\left(\hat{\boldsymbol{\kappa}}_j\right)}$$

for $1\leq j\leq n+1$ in $\boldsymbol{v}\left(\hat{\boldsymbol{\kappa}}_{j+n}\right)$ and for $n+2\leq j\leq N$ in $\boldsymbol{v}\left(\hat{\boldsymbol{\kappa}}_{j-n}\right)$. Thus we have

$$\begin{aligned}
C^N&=-Im\left(\sum_{j=1}^{N}\log<\mathbf{v}\left(\hat{\boldsymbol{\kappa}}_j\right)|\mathbf{v}\left(\hat{\boldsymbol{\kappa}}_{j+1}\right)>\right)\\
&=-Im\left(\sum_{j=1}^{n}\log<\mathbf{v}\left(\hat{\boldsymbol{\kappa}}_j\right)|\mathbf{v}\left(\hat{\boldsymbol{\kappa}}_{j+1}\right)>+\sum_{j=n+1}^{N}\log<\mathbf{v}\left(\hat{\boldsymbol{\kappa}}_j\right)|\mathbf{v}\left(\hat{\boldsymbol{\kappa}}_{j+1}\right)>\right)\\
&=-Im\left(\sum_{j=1}^{n}\log<\overline{\mathbf{v}\left(\hat{\boldsymbol{\kappa}}_{n+j}\right)}|\overline{\mathbf{v}\left(\hat{\boldsymbol{\kappa}}_{n+j+1}\right)}>+\sum_{j=n+1}^{N}\log<\mathbf{v}\left(\hat{\boldsymbol{\kappa}}_j\right)|\mathbf{v}\left(\hat{\boldsymbol{\kappa}}_{j+1}\right)>\right)\\
&=-Im\left(\sum_{j=n+1}^{N}\log<\overline{\mathbf{v}\left(\hat{\boldsymbol{\kappa}}_j\right)}|\overline{\mathbf{v}\left(\hat{\boldsymbol{\kappa}}_{j+1}\right)}>+\sum_{j=n+1}^{N}\log<\mathbf{v}\left(\hat{\boldsymbol{\kappa}}_j\right)|\mathbf{v}\left(\hat{\boldsymbol{\kappa}}_{j+1}\right)>\right)\\
&=-Im\left(\sum_{j=n+1}^{N}\overline{\log<\mathbf{v}\left(\hat{\boldsymbol{\kappa}}_j\right)|\mathbf{v}\left(\hat{\boldsymbol{\kappa}}_{j+1}\right)>}+\sum_{j=n+1}^{N}\log<\mathbf{v}\left(\hat{\boldsymbol{\kappa}}_j\right)|\mathbf{v}\left(\hat{\boldsymbol{\kappa}}_{j+1}\right)>\right)\\
&=0.
\end{aligned}$$

(ii) By Remark 1, $d\left(K_1\right)=d\left(K_3\right)=d\left(K_5\right)$. Therefore, $\mathbf{v}\left(K_1\right)=\mathbf{v}\left(K_3\right)=\mathbf{v}\left(K_5\right)$ which implies $C_{K_1}^N=C_{K_3}^N=C_{K_5}^N$. Similarly, $C_{K_2}^N=C_{K_4}^N=C_{K_6}^N$. Let $\left\{\boldsymbol{\kappa}_j\right\}_{j=1}^N$ be the equally spaced points on the circle as given in the definition of the discrete valley Chern number, wherein $N=2n$ for some $n\in\mathbb{Z}^+$. Note that $arg\left(\boldsymbol{\kappa}_{j+n}\right)=arg\left(\boldsymbol{\kappa}_j\right)+\pi$ for $j=1,2,...,n$, thus

$$K_4 + \boldsymbol{\kappa}_{j+n} = -\left(K_1 + \boldsymbol{\kappa}_j\right) \text{ for } 1 \le j \le n,\ K_4 + \boldsymbol{\kappa}_{j-n} = -\left(K_1 + \boldsymbol{\kappa}_j\right) \text{ for } n+1 \le j \le N. \tag{3.13}$$

Then,

$$d\left(K_4 + \boldsymbol{\kappa}_{j+n}\right) = \overline{d\left(K_1 + \boldsymbol{\kappa}_j\right)} \text{ and } d\left(K_4 + \boldsymbol{\kappa}_{j-n}\right) = \overline{d\left(K_1 + \boldsymbol{\kappa}_j\right)},$$

which implies

$$\boldsymbol{v}\left(K_4 + \boldsymbol{\kappa}_{j\pm n}\right) = \overline{\boldsymbol{v}\left(K_1 + \boldsymbol{\kappa}_j\right)} \text{ for } 1 \le j \le n, \text{ and } n+1 \le j \le N.$$

Then

$$
\begin{aligned}
C_4^N &= -\operatorname{Im}\left(\sum_{j=1}^{2n} \log\left\langle \boldsymbol{v}(K_4+\boldsymbol{\kappa}_j)\,\middle|\,\boldsymbol{v}(K_4+\boldsymbol{\kappa}_{j+1})\right\rangle\right) \\
&= -\operatorname{Im}\Bigg(\sum_{j=1}^{n} \log\left\langle \boldsymbol{v}(K_4+\boldsymbol{\kappa}_j)\,\middle|\,\boldsymbol{v}(K_4+\boldsymbol{\kappa}_{j+1})\right\rangle \\
&\qquad\qquad + \sum_{j=n+1}^{2n} \log\left\langle \boldsymbol{v}(K_4+\boldsymbol{\kappa}_j)\,\middle|\,\boldsymbol{v}(K_4+\boldsymbol{\kappa}_{j+1})\right\rangle\Bigg) \\
&= -\operatorname{Im}\Bigg(\sum_{m=n+1}^{2n} \log\left\langle \boldsymbol{v}(K_4+\boldsymbol{\kappa}_{m-n})\,\middle|\,\boldsymbol{v}(K_4+\boldsymbol{\kappa}_{m-n+1})\right\rangle \\
&\qquad\qquad + \sum_{m=1}^{n} \log\left\langle \boldsymbol{v}(K_4+\boldsymbol{\kappa}_{m+n})\,\middle|\,\boldsymbol{v}(K_4+\boldsymbol{\kappa}_{m+n+1})\right\rangle\Bigg) \\
&= -\operatorname{Im}\Bigg(\sum_{m=n+1}^{2n} \log\left\langle \boldsymbol{v}^*(K_1+\boldsymbol{\kappa}_{m})\,\middle|\,\boldsymbol{v}^*(K_1+\boldsymbol{\kappa}_{m+1})\right\rangle \\
&\qquad\qquad + \sum_{m=1}^{n} \log\left\langle \boldsymbol{v}^*(K_1+\boldsymbol{\kappa}_{m})\,\middle|\,\boldsymbol{v}^*(K_1+\boldsymbol{\kappa}_{m+1})\right\rangle\Bigg) \\
&= -\operatorname{Im}\left(\left[\sum_{m=1}^{2n} \log\left\langle \boldsymbol{v}(K_1+\boldsymbol{\kappa}_{m})\,\middle|\,\boldsymbol{v}(K_1+\boldsymbol{\kappa}_{m+1})\right\rangle\right]^*\right) \\
&= -C_1^N.
\end{aligned}
$$

(iii) Let $\{\boldsymbol{\kappa}_j\}_{j=1}^{N}$ be as in (ii). Then we have

$$
\langle \boldsymbol{v}(\boldsymbol{\kappa}_j)\,|\boldsymbol{v}(\boldsymbol{\kappa}_{j+1})\rangle = (1-\beta)\,|d(\boldsymbol{\kappa}_j)\,||d(\boldsymbol{\kappa}_{j+1})\,|f_j(\beta)\left[r_j(\beta)\,e^{i(\xi_j-\xi_{j+1})}+1\right],
$$

where

$$
\begin{aligned}
f_j(\beta) &= \frac{\left(3\beta+\sqrt{9\beta^2+(1-\beta^2)\,|d(\boldsymbol{\kappa}_j)\,|^2}\right)\left(3\beta+\sqrt{9\beta^2+(1-\beta^2)\,|d(\boldsymbol{\kappa}_{j+1})\,|^2}\right)}{|d(\boldsymbol{\kappa}_j)\,||d(\boldsymbol{\kappa}_{j+1})\,|}, \\
r_j(\beta) &= \frac{1-\beta^2}{f_j(\beta)},\;\; \xi_j = arg\left(d(\boldsymbol{\kappa}_j)\right).
\end{aligned}
$$

For $\beta > 0$, $f_j(\beta) \in [1, \frac{36}{|d(\boldsymbol{\kappa}_j)||d(\boldsymbol{\kappa}_{j+1})|}]$ is an increasing function of β and

$$\sqrt{1-\beta^2}\left|d\left(\boldsymbol{\kappa}_j\right)\right| > 3\beta + \sqrt{9\beta^2 + \left(1-\beta^2\right)\left|d\left(\boldsymbol{\kappa}_j\right)\right|^2},$$

thus $r_j(\beta) \in [0,1]$. Consequently,

$$Im\left(\sum_{j=1}^{N}\log\langle \boldsymbol{v}\left(\boldsymbol{\kappa}_j\right), \boldsymbol{v}\left(\boldsymbol{\kappa}_{j+1}\right)\rangle\right) = Im\left(\sum_{j=1}^{N}\log\left(r_j(\beta)\, e^{i(\xi_j-\xi_{j+1})}+1\right)\right) = \sum_{j=1}^{N}\varepsilon_j, \quad (3.14)$$

where $\varepsilon_j \in \left(0, \frac{\xi_j-\xi_{j+1}}{2}\right)$ and we have used Lemma 1. Denoting $d(\boldsymbol{\kappa}(\theta))$ as $d(\theta)$, it follows that

$$d\left(-\frac{\pi}{3}-\tilde{\theta}\right) = \overline{d\left(-\frac{\pi}{3}+\tilde{\theta}\right)} \text{ and } d\left(\frac{2\pi}{3}-\tilde{\theta}\right) = \overline{d\left(\frac{2\pi}{3}+\tilde{\theta}\right)},$$

for $\tilde{\theta} \in [0, \frac{2\pi}{3}]$ and $\tilde{\theta} \in [0, \frac{\pi}{3}]$ respectively. In addition, $d(-\pi/3)d(2\pi/3) < 0$. Therefore, as $\theta \in [-\pi, \pi]$, $d(\theta)$ surrounds the origin on the complex plane and $arg\left(d\left(-\pi\right)\right) = arg\left(d\left(\pi\right)\right) + 2\pi$. Then, by (3.14),

$$Im\left(\sum_{j=1}^{N}\log\langle \boldsymbol{v}\left(\boldsymbol{\kappa}_j\right), \boldsymbol{v}\left(\boldsymbol{\kappa}_{j+1}\right)\rangle\right) < \sum_{j=1}^{N}\frac{\xi_j-\xi_{j+1}}{2} = \frac{\xi_1-\xi_{N+1}}{2} = \pi.$$

Therefore,

$$Im\left(\sum_{j=1}^{N}\log\langle \boldsymbol{v}\left(\boldsymbol{\kappa}_j\right), \boldsymbol{v}\left(\boldsymbol{\kappa}_{j+1}\right)\rangle\right) \in (0, \pi). \quad (3.15)$$

For $\beta < 0$, there holds $r_j(\beta) > 1$. By similar calculations, we obtain

$$Im\left(\sum_{j=1}^{N}\log\langle \boldsymbol{v}\left(\boldsymbol{\kappa}_j\right), \boldsymbol{v}\left(\boldsymbol{\kappa}_{j+1}\right)\rangle\right) \in (\pi, 3\pi). \quad (3.16)$$

The statement (iii) follows from (3.12), (3.15) and (3.16). □

3.2 Edge Modes for the Topological Mechanical System

We consider a joint system formed by gluing two periodic hexagonal lattices with opposite β values. It forms an interface parallel to $\mathbf{a}_2$ where two identical masses are connected as shown in Figure B.2. For $p \in \mathbb{Z}^+$ and $q \in \mathbb{Z}$, the governing equations for the displacements of the masses located at the left and right sides of the interface are

$$\begin{aligned} m_a \left(U^a_{-p,q}\right)'' + k\left(U^a_{-p,q} - U^b_{-p,q}\right) - k\left(U^a_{-p,q} - U^b_{-(p-1),q}\right) \\ - k\left(U^a_{-p,q} - U^b_{-p,q+1}\right) = 0, \\ m_b \left(U^b_{-(p-1),q}\right)'' + k\left(U^b_{-(p-1),q} - U^a_{-(p-1),q-1}\right) - k\left(U^b_{-(p-1),q} - U^a_{-(p-1),q}\right) \\ - k\left(U^b_{-(p-1),q} - U^a_{-p,q}\right) = 0, \end{aligned} \tag{3.17}$$

and

$$\begin{aligned} m_a \left(U^a_{p,q}\right)'' + k\left(U^a_{p,q} - U^b_{p-1,q}\right) + k\left(U^a_{p,q} - U^b_{p,q-1}\right) + k\left(U^a_{p,q} - U^b_{p,q}\right) = 0, \\ m_b \left(U^b_{p-1,q}\right)'' + k\left(U^b_{p-1,q} - U^a_{p-1,q}\right) + k\left(U^b_{p-1,q} - U^a_{p,q}\right) + k\left(U^b_{p-1,q} - U^a_{p-1,q+1}\right) = 0, \end{aligned} \tag{3.18}$$

respectively. The governing equations for the displacement of the masses located at the interface are

$$\begin{aligned} m_a \left(U^a_{1,q}\right)'' + k\left(U^a_{1,q} - U^a_{-1,q}\right) + k\left(U^a_{1,q} - U^b_{1,q-1}\right) + k\left(U^a_{1,q} - U^b_{1,q}\right) = 0, \\ m_a \left(U^a_{-1,q}\right)'' + k\left(U^a_{-1,q} - U^a_{1,q}\right) + k\left(U^a_{-1,q} - U^b_{-1,q+1}\right) + k\left(U^a_{-1,q} - U^b_{-1,q}\right) = 0. \end{aligned} \tag{3.19}$$

For each $k_{||} \in [0, \frac{2\pi}{a}]$, we consider the solutions that propagate along the interface and decay along the horizontal direction by letting

$$U^a_{p,q}(t) = u^a_p e^{i\omega\gamma} e^{ik_{||}q} \text{ and } U^b_{p,q}(t) = u^b_p e^{i\omega\gamma} e^{ik_{||}q}, \tag{3.20}$$

where $\gamma = \sqrt{k/m}t$. An edge mode $(U^a_{p,q}(t), U^b_{p,q}(t))$ is the nontrivial solution to (3.17) - (3.19) which decays to zero as $p \to \infty$.

We aim to show that there exist edge modes for the joint system in Figure B.2 when $\beta \neq 0$. For each $k_{||} \in [0, \frac{2\pi}{a}]$, such an edge mode attains an eigenfrequency $\omega\left(k_{||}\right)$ such that $\omega^2\left(k_{||}\right)$ is located in the band gap $(\lambda_-\left(k_{||}\right), \lambda_+\left(k_{||}\right))$, where

$$\lambda_-\left(k_{||}\right) = \max_{\tilde{\boldsymbol{\kappa}}} \lambda_-\left(\tilde{\boldsymbol{\kappa}}\right) \text{ and } \lambda_+\left(k_{||}\right) = \min_{\tilde{\boldsymbol{\kappa}}} \lambda_+\left(\tilde{\boldsymbol{\kappa}}\right). \tag{3.21}$$

In the above, $\tilde{\boldsymbol{\kappa}} = k_1 \boldsymbol{b}_1 + \frac{k_{||}a^2}{2\pi}\boldsymbol{b}_2$ and $k_1 \in (0,1)$.

Remark 4. To find $\lambda_\pm\left(k_{||}\right)$, for $k_{||} \in [0, \frac{2\pi}{a}]$, we observe that

$$\begin{aligned}
|d\left(\tilde{\boldsymbol{\kappa}}\right)|^2 &= |-1 - e^{i\tilde{\boldsymbol{\kappa}}\cdot\boldsymbol{a}_1} - e^{i\tilde{\boldsymbol{\kappa}}\cdot\boldsymbol{a}_2}|^2 \\
&= |-1 - e^{i2\pi k_1} - e^{ik_{||}a^2}|^2 \\
&= \left(1 + \cos\left(2\pi k_1\right) + \cos\left(k_{||}a^2\right)\right)^2 + \left(\sin\left(2\pi k_1\right) + \sin\left(k_{||}a^2\right)\right)^2 \\
&= 1 + \cos^2\left(2\pi k_1\right) + \cos^2\left(k_{||}a^2\right) + 2\cos\left(2\pi k_1\right) + 2\cos\left(k_{||}a^2\right) \\
&\quad + 2\cos\left(2\pi k_1\right)\cos\left(k_{||}a^2\right) + \sin^2\left(2\pi k_1\right) + 2\sin\left(2\pi k_1\right)\sin\left(k_{||}a^2\right) + \sin^2\left(k_{||}a^2\right) \\
&= 3 + 2\cos\left(k_{||}a^2\right) + 2\cos\left(2\pi k_1\right) + 2\cos\left(2\pi k_1 - k_{||}a^2\right) \\
&= 3 + 2\cos\left(k_{||}a^2\right) + 4\cos\left(\frac{2\pi k_1 + 2\pi k_1 - k_{||}a^2}{2}\right)\cos\left(\frac{2\pi k_1 - 2\pi k_1 + k_{||}a^2}{2}\right) \\
&= 3 + 2\cos\left(k_{||}a^2\right) + 4\cos\left(2\pi k_1 - \frac{k_{||}a^2}{2}\right)\cos\left(\frac{k_{||}a^2}{2}\right).
\end{aligned} \tag{3.22}$$

Define $g\left(k_1\right) = \lambda_+\left(\tilde{\boldsymbol{\kappa}}\right)$. We have

$$0 = g'\left(k_1\right) = \frac{1}{2}\left(\frac{9\beta^2}{\left(1-\beta^2\right)^2} + \frac{|d\left(\tilde{\boldsymbol{\kappa}}\right)|^2}{1-\beta^2}\right)^{-1/2} \frac{\frac{d}{dk_1}(|d\left(\tilde{\boldsymbol{\kappa}}\right)|^2)}{1-\beta^2},$$

which is equivalent to, by (3.22),

$$0 = \frac{d}{dk_1}(|d\left(\tilde{\boldsymbol{\kappa}}\right)|^2) = -8\pi\sin\left(2\pi k_1 - \frac{k_{||}a^2}{2}\right)\cos\left(\frac{k_{||}a^2}{2}\right).$$

Then $g\left(k_1\right)$ attains its extreme values when

$$k_1 = \frac{n}{2} + \frac{k_{||}a^2}{4\pi}$$

Also, by letting $\tilde{\boldsymbol{\kappa}}_1 = \frac{n}{2} + \frac{k_{||}a^2}{4\pi}\boldsymbol{b}_1 + \frac{k_{||}a^2}{2\pi}\boldsymbol{b}_2$, we have

$$\begin{aligned}
\frac{d^2}{d(k_1)^2}(|d\left(\tilde{\boldsymbol{\kappa}}\right)|^2)|_{\tilde{\boldsymbol{\kappa}}=\tilde{\boldsymbol{\kappa}}_1} &= -16\pi^2 \cos\left(2\pi\left(\frac{n}{2} + \frac{k_{||}a^2}{4\pi}\right) - \frac{k_{||}a^2}{2}\right)\cos\left(\frac{k_{||}a^2}{2}\right) \\
&= -16\pi^2 \cos\left(n\pi\right)\cos\left(\frac{k_{||}a^2}{2}\right) \\
&= -16\pi^2(-1)^n \cos\left(\frac{k_{||}a^2}{2}\right).
\end{aligned}$$

Thus, we conclude that $\lambda_-\left(k_{||}\right)$ and $\lambda_+\left(k_{||}\right)$ occur when

$$\tilde{\boldsymbol{\kappa}} = \left(\frac{n}{2} + \frac{k_{||}a^2}{4\pi}\right)\boldsymbol{b}_1 + \frac{k_{||}a^2}{2\pi}\boldsymbol{b}_2, \text{ for } n \in \{0, 1\},$$

with $(-1)^n \cos\left(\frac{k_{||}a^2}{2}\right) < 0$ and we have

$$\lambda_-\left(k_{||}\right) = \frac{3 - \sqrt{9\beta^2 + (1-\beta^2)\left|d\left(\tilde{\boldsymbol{\kappa}_1}\right)\right|^2}}{1-\beta^2} \text{ and } \lambda_+\left(k_{||}\right) = \frac{3 + \sqrt{9\beta^2 + (1-\beta^2)\left|d\left(\tilde{\boldsymbol{\kappa}_1}\right)\right|^2}}{1-\beta^2}, \tag{3.23}$$

where

$$
\begin{aligned}
|d(\tilde{\boldsymbol{\kappa}}_1)| &= \left(3+2\cos\left(k_{||}a^2\right)+4\cos\left(2\pi\left(\frac{n}{2}+\frac{k_{||}a^2}{4\pi}\right)-\frac{k_{||}a^2}{2}\right)\cos\left(\frac{k_{||}a^2}{2}\right)\right)^{1/2} \\
&= \left(3+2\cos\left(k_{||}a^2\right)+4\cos(n\pi)\cos\left(\frac{k_{||}a^2}{2}\right)\right)^{1/2} \\
&= \left(3+2\left(2\cos^2\left(\frac{k_{||}a^2}{2}\right)-1\right)+4(-1)^n\cos\left(\frac{k_{||}a^2}{2}\right)\right)^{1/2} \\
&= \left(1+(-1)^n 4\cos\left(\frac{k_{||}a^2}{2}\right)+4\cos^2\left(\frac{k_{||}a^2}{2}\right)\right)^{1/2} \\
&= \left(\left(1+(-1)^n 2\cos\left(\frac{k_{||}a^2}{2}\right)\right)^2\right)^{1/2}
\end{aligned}
$$

Thus,

$$
|d(\tilde{\boldsymbol{\kappa}}_1)| = \left|1+(-1)^n\, 2\cos\left(\frac{k_{||}a^2}{2}\right)\right|. \tag{3.24}
$$

It is also clear that $\lambda_-\left(k_{||}\right) < \lambda_+\left(k_{||}\right)$.

Our main result is stated in the following theorem.

Theorem 2. (Existence of edge modes) If two periodic systems with opposite β values are connected as in Figure B.1(b), then for each $k_{||} \in [0, \frac{2\pi}{a}]$, there exist two interface modes in the form (3.20) with $\omega^2_{1,2}\left(k_{||}\right) \in (\lambda_-\left(k_{||}\right), \lambda_+\left(k_{||}\right))$.

Remark 5. By Lemma 3, if β_1 and β_2 attain opposite signs, then $C^{(1)}_{K_j} C^{(2)}_{K_j} < 0$ where $C^{(i)}_{K_j}$ is the valley Chern number calculated with β_i at K_j.

3.2.1 Transfer Matrix for the Periodic System

In this subsection, we compute the transfer matrices for the lattices on the left and right sides of the interface. To simplify the calculations, we introduce the following notations:

$$\begin{aligned}
\tau\left(k_{||}\right) &:= 3-(1+\beta)\omega^2\left(k_{||}\right),\\
\sigma\left(k_{||}\right) &:= 3-(1-\beta)\omega^2\left(k_{||}\right),\\
z\left(k_{||}\right) &:= 1+e^{ik_{||}a^2},\\
\xi\left(\sigma,k_{||}\right) &:= \tau\sigma-1-|z|^2,
\end{aligned}$$

We consider the solutions in the form of (3.20) for (3.17)-(3.19). For the right periodic system, by (3.18),

$$\begin{aligned}
m(1+\beta)\frac{k}{m}(-\omega^2)u_p^a e^{i(\omega+\gamma+k_{||}q)}+k\left(3u_p^a-u_p^b-u_{p-1}^b-u_p^b e^{-ik_{||}}\right)e^{i(\omega+\gamma+k_{||}q)} &= 0\\
m(1-\beta)\frac{k}{m}(-\omega^2)u_{p-1}^b e^{i(\omega+\gamma+k_{||}q)}+k\left(3u_{p-1}^b-u_{p-1}^a-u_p^a-u_{p-1}^a e^{ik_{||}}\right)e^{i(\omega+\gamma+k_{||}q)} &= 0.
\end{aligned}$$

Then u_p^a and u_p^b satisfy

$$\begin{aligned}
\tau u_p^a-u_{p-1}^b-u_p^b-u_p^b e^{-ik_{||}a^2} &= 0,\\
\sigma u_{p-1}^b-u_{p-1}^a-u_p^a-u_{p-1}^a e^{ik_{||}a^2} &= 0,
\end{aligned}\tag{3.25}$$

which is reduced to $A\left(k_{||}\right)\mathbf{u}_{p-1}=B\left(k_{||}\right)\mathbf{u}_p$ where

$$A\left(k_{||}\right)=\begin{bmatrix}0 & 1\\ -z\left(k_{||}\right) & \sigma\end{bmatrix},\ B\left(k_{||}\right)=\begin{bmatrix}\tau & -\overline{z\left(k_{||}\right)}\\ 1 & 0\end{bmatrix}\ \text{and}\ \mathbf{u}_p=\begin{bmatrix}u_p^a\\ u_p^b\end{bmatrix}=\begin{bmatrix}u^a\\ u^b\end{bmatrix}_p.$$

We rewrite $A\mathbf{u}_{p-1}=B\mathbf{u}_p$ as

$$T_R\left(k_{||}\right)\mathbf{u}_{p-1}=\mathbf{u}_p,$$

where the transfer matrix

$$T_R\left(k_{||}\right) = B^{-1}A = \frac{1}{\overline{z}} \begin{bmatrix} 0 & \overline{z\left(k_{||}\right)} \\ -1 & \tau \end{bmatrix} \begin{bmatrix} 0 & 1 \\ -z\left(k_{||}\right) & \sigma \end{bmatrix} = \frac{1}{\overline{z}} \begin{bmatrix} -|z|^2 & \overline{z}\sigma \\ -z\tau & \tau\sigma - 1 \end{bmatrix},$$

with its characteristic equation

$$\lambda^2 - \frac{1}{\overline{z}}\left(\tau\rho - 1 - |z|^2\right)\lambda + \frac{z}{\overline{z}} = 0.$$

Then, the eigenpairs of T_R are

$$\lambda_{R,\pm}\left(k_{||}\right) = \frac{1}{2\overline{z}}\left[\xi \pm \sqrt{\xi^2 - 4|z|^2}\right] \text{ and } \mathbf{v}_{R,\pm}\left(k_{||}\right) = \begin{bmatrix} \sigma \\ \lambda_{R,\pm} + z \end{bmatrix}.$$

Similarly, by (3.17), u^a_{-p} and u^b_{-p} satisfy

$$\tau u^a_{-p} - u^b_{-p} - u^b_{-(p-1)} - e^{ik_{||}a^2} u^b_{-p} = 0,$$
$$\tau u^b_{-(p-1)} - u^a_{-(p-1)} - u^a_{-(p-1)} - e^{-ik_{||}a^2} u^a_{-p} = 0.$$

We obtain $T_L\left(k_{||}\right)\mathbf{u}_{-p} = \mathbf{u}_{-(p+1)}$, where the transfer matrix

$$T_L\left(k_{||}\right) = \frac{1}{z} \begin{bmatrix} -|z|^2 & z\sigma \\ -\overline{z}\tau & \tau\sigma - 1 \end{bmatrix}.$$

Since $T_R = \overline{T_L}$, the eigenpairs of T_L are

$$\lambda_{L,\pm}\left(k_{||}\right) = \overline{\lambda_{R,\pm}\left(k_{||}\right)} = \frac{1}{2z}\left[\xi \pm \sqrt{\xi^2 - 4|z|^2}\right] \text{ and } \mathbf{v}_{L,\pm}\left(k_{||}\right) = \overline{\mathbf{v}_{R,\pm}\left(k_{||}\right)} = \begin{bmatrix} \sigma \\ \lambda_{L,\pm} + \overline{z} \end{bmatrix}.$$

Remark 6. Along the interface, we have

$$\begin{aligned}
|z|^2 &= \left|1 + e^{ik_{||}a^2}\right|^2 \\
&= \left(1 + \cos\left(k_{||}a^2\right)\right)^2 + \sin^2\left(k_{||}a^2\right) \\
&= 2 + 2\cos\left(k_{||}a^2\right) \\
&= \left((-1)^{n+1} 2\cos\left(\frac{k_{||}a^2}{2}\right)\right)^2,
\end{aligned}$$

since, by Remark 4, $(-1)^n 2\cos\left(\frac{k_{||}a^2}{2}\right) < 0$. Then, by (3.24),

$$|d|^2 = \left|1 + (-1)^n 2\cos\left(\frac{k_{||}a^2}{2}\right)\right|^2 = (1 - |z|)^2$$

In order for $\mathbf{u}_p$ to decay as $p \to \pm\infty$, it is necessary that $\mathbf{u}_1 = \begin{bmatrix} u^a \\ u^b \end{bmatrix}_1$ and $\mathbf{u}_{-1} = \begin{bmatrix} u^a \\ u^b \end{bmatrix}_{-1}$ are parallel to the eigenvectors of T_R and T_L whose corresponding eigenvalues have absolute value less than 1.

Remark 7. (i) If $\xi^2 - 4|z|^2 < 0$, then

$$|\lambda_R|^2 = |\lambda_L|^2 = \frac{1}{4|z|^2}\left|\xi \pm i\sqrt{4|z|^2 - \xi^2}\right|^2 = \frac{1}{4|z|^2}\left(\xi^2 + 4|z|^2 - \xi^2\right) = 1.$$

Since we consider $\left|\lambda_{L,R}\right| < 1$, there holds $\xi^2 - 4|z|^2 \geq 0$ and

$$\begin{aligned}
|\lambda_R|^2 = |\lambda_L|^2 &= \frac{1}{4|z|^2}\left(\xi \pm \sqrt{\xi^2 - 4|z|^2}\right)^2 \\
&= \frac{1}{4|z|^2}\left(\xi^2 \pm 2\xi\sqrt{\xi^2 - 4|z|^2} + \xi^2 - 4|z|^2\right) \\
&= \frac{2\xi^2 - 4|z|^2}{4|z|^2} \pm \frac{2\xi\sqrt{\xi^2 - 4|z|^2}}{4|z|^2}.
\end{aligned}$$

Also, $\xi^2 - 4|z|^2 \geq 0$ gives that

$$\frac{2\xi^2 - 4|z|^2}{4|z|^2} \geq \frac{\xi^2}{4|z|^2} \geq 1.$$

(ii) If $\left|\lambda_{R,+}\right|^2 < 1$, then

$$1 > \left|\lambda_{R,+}\right|^2 = \frac{2\xi^2 - 4|z|^2}{4|z|^2} + \frac{2\xi\sqrt{\xi^2 - 4|z|^2}}{4|z|^2} \geq 1 + \frac{2\xi\sqrt{\xi^2 - 4|z|^2}}{4|z|^2}.$$

Thus,

$$\xi\sqrt{\xi^2 - 4\left|z\right|^2} < 0,$$

which implies $\xi < 0$. If $\left|\lambda_{R,-}\right|^2 < 1$, then, by changing the sign of the second term,

$$-\xi\sqrt{\xi^2 - 4\left|z\right|^2} < 0,$$

which implies $\xi > 0$.

By Remark 7, the eigenvalue λ_R with $|\lambda_R| < 1$ is

$$\lambda_R = \begin{cases} \frac{1}{2\bar{z}}\left(\xi - \sqrt{\xi^2 - 4\left|z\right|^2}\right), & \text{for } \xi > 0, \\ \frac{1}{2\bar{z}}\left(\xi + \sqrt{\xi^2 - 4\left|z\right|^2}\right), & \text{for } \xi < 0. \end{cases} \tag{3.26}$$

Since $\lambda_{L,\pm} = \overline{\lambda_{R,\pm}}$, we have

$$\lambda_L = \begin{cases} \frac{1}{2z}\left(\xi - \sqrt{\xi^2 - 4\left|z\right|^2}\right), & \text{for } \xi > 0, \\ \frac{1}{2z}\left(\xi + \sqrt{\xi^2 - 4\left|z\right|^2}\right), & \text{for } \xi < 0. \end{cases} \tag{3.27}$$

Thus, with (3.26) and (3.27), the parallelism condition above implies that

$$\begin{bmatrix} u_1^a \\ u_1^b \end{bmatrix} = c_1 \mathbf{v}_R = \begin{bmatrix} c_1 \sigma \\ c_1 \left(\lambda_R + z\right) \end{bmatrix} \quad \text{and} \quad \begin{bmatrix} u_{-1}^a \\ u_{-1}^b \end{bmatrix} = c_2 \mathbf{v}_L = \begin{bmatrix} c_2 \sigma \\ c_2 \left(\lambda_L + \overline{z}\right) \end{bmatrix}. \tag{3.28}$$

3.2.2 Proof of Theorem 2

By (3.19) and (3.20), we obtain

$$\begin{aligned} m(1+\beta)(-\omega^2)\frac{k}{m} u_1^a e^{i\left(\omega\tau + k_{\|} q\right)} + k\left(3u_1^a - u_{-1}^a - u_1^b - u_1^b e^{-ik_{\|}}\right) e^{i\left(\omega\tau + k_{\|} q\right)} &= 0, \\ m(1+\beta)(-\omega^2)\frac{k}{m} u_{-1}^a e^{i\left(\omega\tau + k_{\|} q\right)} + k\left(3u_{-1}^a - u_1^a - u_{-1}^b - u_{-1}^b e^{ik_{\|}}\right) e^{i\left(\omega\tau + k_{\|} q\right)} &= 0, \end{aligned}$$

which implies

$$\begin{aligned} \tau u_1^a - u_{-1}^a - \overline{z} u_1^b &= 0, \\ \tau u_{-1}^a - u_1^a - z u_{-1}^b &= 0. \end{aligned} \tag{3.29}$$

Then, by using (3.28), (3.29) can be simplified as

$$\begin{aligned} \tau c_1 \sigma - \overline{z} c_1 \left(\lambda_R z\right) - c_2 \sigma &= 0, \\ \tau c_2 \sigma - z c_2 \left(\lambda_L \overline{z}\right) - c_1 \sigma &= 0. \end{aligned} \tag{3.30}$$

For $\sigma = 0$, the first equation in (3.30) implies that

$$c_1 \lambda_R |z|^2 = 0.$$

which is equivalent to $c_1 = 0$ and it gives the trivial solution for (3.25). Therefore, $\sigma \neq 0$ and

$$c_2 = \frac{1}{\sigma} c_1 \left(\tau\sigma - \overline{z}\left(\lambda_R + z\right)\right), \tag{3.31}$$

(3.31) and the second equation in (3.30) together imply that

$$c_1\sigma = \frac{1}{\sigma}c_1\left(\tau\sigma - \overline{z}\left(\lambda_R + z\right)\right)\left(\tau\sigma - z\left(\lambda_L + \overline{z}\right)\right).$$

Since $\lambda_R = \overline{\lambda_L}$, we have

$$\sigma^2 = \left(\tau\sigma - \overline{z}\left(\lambda_R + z\right)\right)\left(\tau\sigma - z\left(\overline{\lambda_R} + \overline{z}\right)\right) = \left|\tau\sigma - \overline{z}\left(\lambda_R + z\right)\right|^2$$

By (3.26), for $\xi < 0$,

$$\begin{aligned}
\sigma^2 &= \left|\tau\sigma - \overline{z}\left(\lambda_R + z\right)\right|^2 \\
&= \left|\tau\sigma - |z|^2 - \overline{z}\lambda_R\right|^2 \\
&= \left|\xi + 1 - \overline{z}\frac{1}{2\overline{z}}\left(\xi + \sqrt{\xi^2 - 4|z|^2}\right)\right|^2 \\
&= \frac{1}{4}\left|2\xi + 2 - \left(\xi + \sqrt{\xi^2 - 4|z|^2}\right)\right|^2
\end{aligned}$$

By similar calculations for $\xi > 0$, we have

$$4\sigma^2 = \begin{cases} \left|\xi + 2 - \sqrt{\xi^2 - 4|z|^2}\right|^2, & \text{for } \xi < 0, \\ \left|\xi + 2 + \sqrt{\xi^2 - 4|z|^2}\right|^2, & \text{for } \xi > 0, \end{cases} \tag{3.32}$$

by (3.26). We consider $\xi < 0$ and $\xi > 0$ respectively to obtain a solution to (3.32). We have, if $\xi < 0$,

$$2\sigma = \xi + 2 - \sqrt{\xi^2 - 4|z|^2} \text{ or } 2\sigma = -(\xi + 2) + \sqrt{\xi^2 - 4|z|^2}.$$

(i) If $2\sigma = \xi + 2 - \sqrt{\xi^2 - 4|z|^2}$, then

$$\begin{aligned}\xi^2 - 4|z|^2 &= (2\sigma - (\xi+2))^2 \\ &= 4\sigma^2 - 4\sigma(\xi+2) + \xi^2 + 4\xi + 4. \end{aligned} \tag{3.33}$$

Note that $\omega^2 = \frac{3-\sigma}{1-\beta}$ and

$$\tau = 3 - (1+\beta)\frac{3-\sigma}{1-\beta} = \frac{(1+\beta)\sigma - 6\beta}{1-\beta}$$

Then (3.33) becomes

$$\begin{aligned} 0 &= 4\sigma^2 - 4\sigma(\xi+2) + 4\xi + 4|z|^2 + 4 \\ &= 4\left(\sigma^2 - \sigma\left(\tau\sigma - 1 - |z|^2 + 2\right) + \tau\sigma - 1 - |z|^2 + |z|^2 + 1\right) \\ &= 4\sigma\left(\sigma - \tau\sigma + |z|^2 - 1 + \tau\right) \\ &= 4\sigma\left(\sigma - \sigma\frac{(1+\beta)\sigma - 6\beta}{1-\beta} + \frac{(1+\beta)\sigma - 6\beta}{1-\beta} + |z|^2 - 1\right) \\ &= 4\sigma\left(\sigma - \frac{1+\beta}{1-\beta}\sigma^2 + \frac{6\beta}{1-\beta}\sigma + \frac{1+\beta}{1-\beta}\sigma - \frac{6\beta}{1-\beta} + |z|^2 - 1\right) \end{aligned}$$

which implies

$$\sigma\left(-\frac{1+\beta}{1-\beta}\sigma^2 + \left[1 + \frac{6\beta}{1-\beta} + \frac{1+\beta}{1-\beta}\right]\sigma - \left[1 - |z|^2 + \frac{6\beta}{1-\beta}\right]\right) = 0. \tag{3.34}$$

Observe that

$$
\begin{aligned}
&\left(1+\frac{6\beta}{1-\beta}+\frac{1+\beta}{1-\beta}\right)^{2}-4\left(-\frac{1+\beta}{1-\beta}\right)\left(-\left[1-|z|^{2}+\frac{6\beta}{1-\beta}\right]\right) \\
&=\left(\frac{1-\beta+6\beta+1+\beta}{1-\beta}\right)^{2}-4\frac{1+\beta}{1-\beta}\left(1-|z|^{2}+\frac{6\beta}{1-\beta}\right) \\
&=\frac{1}{(1-\beta)^{2}}\left((2+6\beta)^{2}-4(1+\beta)\left(1+5\beta-(1-\beta)|z|^{2}\right)\right) \\
&=\frac{1}{(1-\beta)^{2}}\left(4+24\beta+36\beta^{2}-4(1+\beta)-20\beta(1+\beta)+4\left(1-\beta^{2}\right)|z|^{2}\right) \\
&=\frac{4}{(1-\beta)^{2}}\left(4\beta^{2}+\left(1-\beta^{2}\right)|z|^{2}\right)
\end{aligned}
$$

Thus, (3.34) attains two nonzero roots:

$$
\sigma_{1}=\frac{1+3\beta-\sqrt{4\beta^{2}+\left(1-\beta^{2}\right)|z|^{2}}}{(1+\beta)},\quad \sigma_{2}=\frac{1+3\beta+\sqrt{4\beta^{2}+\left(1-\beta^{2}\right)|z|^{2}}}{(1+\beta)}.
$$

Note that, for $\beta\in(-1,1)$, taking $s=\sqrt{4\beta^{2}+(1-\beta^{2})|z|^{2}}$,

$$
s=\sqrt{4\beta^{2}+(1-\beta^{2})|z|^{2}}\geq 2|\beta|,
$$

and

$$
s^{2}=4\beta^{2}+\left(1-\beta^{2}\right)|z|^{2}.
$$

Thus, we have

$$
\begin{aligned}
\tau\left(\sigma_{1}\right)&=\frac{(1+\beta)\sigma_{1}-6\beta}{1-\beta} \\
&=\frac{(1+\beta)}{1-\beta}\frac{1+3\beta-s}{(1+\beta)}-\frac{6\beta}{1-\beta} \\
&=\frac{1+3\beta-s}{(1-\beta)}-\frac{6\beta}{1-\beta} \\
&=\frac{1-3\beta-s}{(1-\beta)},
\end{aligned}
$$

and

$$
\begin{aligned}
\tau\left(\sigma_2\right) &= \frac{(1+\beta)\sigma_2 - 6\beta}{1-\beta} \\
&= \frac{(1+\beta)}{1-\beta}\frac{1+3\beta+s}{(1+\beta)} - \frac{6\beta}{1-\beta} \\
&= \frac{1+3\beta+s}{(1-\beta)} - \frac{6\beta}{1-\beta} \\
&= \frac{1-3\beta+s}{(1-\beta)}.
\end{aligned}
$$

Then, by using $\tau = \frac{(1+\beta)\sigma}{1-\beta} - \frac{6\beta}{1-\beta}$,

$$
\begin{aligned}
\xi(\sigma_1, k_{||}) &= \left(\frac{1+\beta}{1-\beta}\sigma_1 - \frac{6\beta}{1-\beta}\right)\sigma_1 - |z|^2 - 1 \\
&= \frac{1+\beta}{1-\beta}\left(\frac{1+3\beta-s}{1+\beta}\right)^2 - \frac{6\beta}{1-\beta}\frac{1+3\beta-s}{1+\beta} - |z|^2 - 1 \\
&= \frac{1+6\beta+9\beta^2+2s\left(1+3\beta\right)+s^2-6\beta\left(1+3\beta\right)+6\beta s-\left(1-\beta^2\right)|z|^2-\left(1-\beta^2\right)}{1-\beta^2} \\
&= -\frac{4\beta^2+2s}{1-\beta^2} \\
&< 0,
\end{aligned}
$$

but

$$
\begin{aligned}
\xi(\sigma_2, k_{||}) &= \frac{1-3\beta+s}{(1-\beta)}\frac{1+3\beta+s}{(1+\beta)} - |z|^2 - 1 \\
&= \frac{1}{1-\beta^2}\left(1-9\beta^2+(1-3\beta)\,s+(1+3\beta)\,s+s^2\right) - |z|^2 - 1 \\
&= \frac{1}{1-\beta^2}\left(1-9\beta^2+(1-3\beta)\,s+(1+3\beta)\,s+4\beta^2+\left(1-\beta^2\right)|z|^2\right) - |z|^2 - 1 \\
&= \frac{1-5\beta^2+2s-\left(1-\beta^2\right)}{1-\beta^2}\,() + |z|^2 - |z|^2 \\
&= \frac{-4\beta^2+2s}{1-\beta^2} \\
&\geq 4\frac{|\beta|-\beta^2}{1-\beta^2} \\
&> 0
\end{aligned}
$$

which is a contradiction to $\xi < 0$. Therefore,

$$
\tilde{\sigma}_1 = \frac{1+3\beta-\sqrt{4\beta^2+(1-\beta^2)\,|z|^2}}{(1+\beta)}
$$

is one root of (3.34).

(ii) If $2\sigma = -(\xi+2)+\sqrt{\xi^2-4\,|z|^2}$, by similar calculations, we obtain two more roots

$$
\sigma_3 = \frac{-1+3\beta+\sqrt{16\beta^2+(1-\beta^2)\,|z|^2}}{1+\beta}, \text{ and } \sigma_4 = \frac{-1+3\beta-\sqrt{16\beta^2+(1-\beta^2)\,|z|^2}}{1+\beta}.
$$

Similarly, we have

$$
\xi\left(\sigma_3, k_{||}\right) = \frac{8\beta^2-2\sqrt{16\beta^2+(1-\beta^2)\,|z|^2}}{1-\beta^2} \leq 8\frac{\beta^2-|\beta|}{1-\beta^2} \leq 0,
$$

but

$$
\xi\left(\sigma_4, k_{||}\right) = 2\frac{4\beta^2+4\,|\beta|}{1-\beta^2} \geq 0.
$$

Thus, we obtain

$$\tilde{\sigma}_2 = \frac{-1+3\beta+\sqrt{16\beta^2+(1-\beta^2)\left|z\right|^2}}{1+\beta},$$

as another root of (3.32).

By similar calculations for $\xi > 0$, we obtain two more roots:

$$\tilde{\sigma}_3 = \frac{1+3\beta+\sqrt{4\beta^2+(1-\beta^2)\left|z\right|^2}}{1+\beta} \text{ and } \tilde{\sigma}_4 = \frac{-1+3\beta-\sqrt{16\beta^2+(1-\beta^2)\left|z\right|^2}}{1+\beta}.$$

From the relation $\sigma = 3-(1-\beta)\,\omega^2$, we have

$$\begin{aligned}
\omega_1^2\left(\tilde{\sigma}_1, k_{||}\right) &= \frac{3-\tilde{\sigma}_1}{1-\beta} \\
&= \frac{1}{1-\beta}\left(3-\frac{1+3\beta-\sqrt{4\beta^2+(1-\beta^2)\left|z\right|^2}}{(1+\beta)}\right) \\
&= \frac{2+\sqrt{4\beta^2+(1-\beta^2)\left|z\right|^2}}{1-\beta^2}.
\end{aligned}$$

By similar calculations, we obtain the corresponding eigenvalues:

$$\begin{aligned}
\omega_1^2\left(k_{||}\right) &= \frac{2+\sqrt{4\beta^2+(1-\beta^2)\left|z\right|^2}}{1-\beta^2}, \\
\omega_2^2\left(k_{||}\right) &= \frac{4-\sqrt{16\beta^2+(1-\beta^2)\left|z\right|^2}}{1-\beta^2}, \\
\omega_3^2\left(k_{||}\right) &= \frac{2-\sqrt{4\beta^2+(1-\beta^2)\left|z\right|^2}}{1-\beta^2}, \\
\omega_4^2\left(k_{||}\right) &= \frac{4+\sqrt{16\beta^2+(1-\beta^2)\left|z\right|^2}}{1-\beta^2}.
\end{aligned} \tag{3.35}$$

Next we show that $\omega_j^2\left(k_{||}\right) \in \left(\lambda_-\left(k_{||}\right), \lambda_+\left(k_{||}\right)\right)$ for $j = 1, 2$ but $\omega_j^2\left(k_{||}\right) \notin \left(\lambda_-\left(k_{||}\right), \lambda_+\left(k_{||}\right)\right)$

for $j = 3, 4$. We have

$$\sqrt{4\beta^2 + (1-\beta^2)|z|^2} = \sqrt{|z|^2 + \beta^2 (4 - |z|^2)} \geq \sqrt{|z|^2} = |z|,$$

and

$$\begin{aligned}
\sqrt{9\beta^2 + (1-\beta^2)|d|^2} &= \sqrt{9\beta^2 + (1-\beta^2)(1-|z|)^2} \\
&= \sqrt{(1-|z|)^2 + \beta^2 \left(9 - (1-|z|)^2\right)} \\
&\geq \sqrt{(1-|z|)^2} \\
&\geq 1 - |z|.
\end{aligned}$$

Then

$$\begin{aligned}
w_1^2 - \lambda_- &= \frac{2 + \sqrt{4\beta^2 + (1-\beta^2)|z|^2}}{1-\beta^2} - \frac{3 - \sqrt{9\beta^2 + (1-\beta^2)|d|^2}}{1-\beta^2} \\
&= \frac{\sqrt{4\beta^2 + (1-\beta^2)|z|^2} + \sqrt{9\beta^2 + (1-\beta^2)|d|^2} - 1}{1-\beta^2} \geq \frac{|z| + 1 - |z| - 1}{1-\beta^2} \\
&= 0
\end{aligned}$$

Thus, $\omega_1^2 \geq \lambda_-$. For the upper bound, we have

$$\begin{aligned}
1 + 2\beta^2 + \sqrt{9\beta^2 + (1-\beta^2)|d|^2} &= 1 + 2\beta^2 + \sqrt{9\beta^2 + (1-\beta^2)|1-|z||^2} \\
&\geq 1 + 2\beta^2 + \sqrt{9\beta^2 + (1-\beta^2)} \\
&= 1 + 2\beta^2 + \sqrt{8\beta^2 + 1} \\
&\geq 2 + 2\beta^2 \\
&\geq 2 - 2\beta^2 \\
&= \left(1-\beta^2\right) 2 \\
&\geq \left(1-\beta^2\right)|z|.
\end{aligned}$$

Thus,

$$
\begin{aligned}
0 &\leq 2+4\beta^2+2\sqrt{9\beta^2+\left(1-\beta^2\right)|d|^2}-2\left(1-\beta^2\right)|z| \\
&= 2+4\beta^2+2\sqrt{9\beta^2+\left(1-\beta^2\right)|d|^2}-2\left(1-\beta^2\right)|z|+4\beta^2+\left(1-\beta^2\right)|z|^2 \\
&\qquad\qquad -\left(4\beta^2+\left(1-\beta^2\right)|z|^2\right) \\
&= 2+8\beta^2+2\sqrt{9\beta^2+\left(1-\beta^2\right)|d|^2}-2\left(1-\beta^2\right)|z|+\left(1-\beta^2\right)|z|^2-\left(4\beta^2+\left(1-\beta^2\right)|z|^2\right) \\
&= 1+9\beta^2+2\sqrt{9\beta^2+\left(1-\beta^2\right)|d|^2}+1-\beta^2-2\left(1-\beta^2\right)|z|+\left(1-\beta^2\right)|z|^2 \\
&\qquad\qquad -\left(4\beta^2+\left(1-\beta^2\right)|z|^2\right) \\
&= 1+2\sqrt{9\beta^2+\left(1-\beta^2\right)|d|^2}+9\beta^2+\left(1-\beta^2\right)\left(1-2|z|+|z|^2\right)-\left(4\beta^2+\left(1-\beta^2\right)|z|^2\right) \\
&= 1+2\sqrt{9\beta^2+\left(1-\beta^2\right)|d|^2}+9\beta^2+\left(1-\beta^2\right)|d|^2-\left(4\beta^2+\left(1-\beta^2\right)|z|^2\right) \\
&= 1+2\sqrt{9\beta^2+\left(1-\beta^2\right)|d|^2}+\left(\sqrt{9\beta^2+\left(1-\beta^2\right)|d|^2}\right)^2-\left(4\beta^2+\left(1-\beta^2\right)|z|^2\right) \\
&= \left(1+\sqrt{9\beta^2+\left(1-\beta^2\right)|d|^2}\right)^2-\left(4\beta^2+\left(1-\beta^2\right)|z|^2\right).
\end{aligned}
$$

Then

$$
1+\sqrt{9\beta^2+\left(1-\beta^2\right)|d|^2} \geq \sqrt{4\beta^2+\left(1-\beta^2\right)|z|^2} \tag{3.36}
$$

By using (3.36), we get

$$
\begin{aligned}
w_1^2-\lambda_+ &= \frac{2+\sqrt{4\beta^2+\left(1-\beta^2\right)|z|^2}}{1-\beta^2}-\frac{3+\sqrt{9\beta^2+\left(1-\beta^2\right)|d|^2}}{1-\beta^2} \\
&= \frac{\sqrt{4\beta^2+\left(1-\beta^2\right)|z|^2}-1-\sqrt{9\beta^2+\left(1-\beta^2\right)|d|^2}}{1-\beta^2} \\
&\leq 0.
\end{aligned}
$$

Thus, $\omega_1^2 \leq \lambda_+$ and we have $\omega_1^2 \in [\lambda_-, \lambda_+]$. By similar calculations, we can show $\omega_2^2 \in [\lambda_-, \lambda_+]$. To show $\omega_3^2 \notin [\lambda_-, \lambda_+]$, we have the following remarks.

Remark 8. For $u \in [0,1]$,

$$\begin{aligned}
0 &\geq u^2 - u \\
&= 4u^2 - 4u \\
&= 1 + 8u^2 - \left(1 + 4u + 4u^2\right) \\
&= 1 + 8u^2 - \left(1 + 2u\right)^2 \\
&= \left(\sqrt{1 + 8u^2} - (1 + 2u)\right)\left(\sqrt{1 + 8u^2} + (1 + 2u)\right)
\end{aligned}$$

Thus, $\sqrt{1 + 8u^2} - (1 + 2u) \leq 0$ and

$$\sqrt{1 + 8u^2} - 2u \leq 1$$

Remark 9. Define

$$F(t) = \sqrt{9\beta^2 + \left(1 - \beta^2\right)\left(1 - t\right)^2} - \sqrt{4\beta^2 + \left(1 - \beta^2\right)t^2}.$$

For $0 \leq t \leq 1$,

$$F'(t) = \frac{-\left(1 - \beta^2\right)\left(1 - t\right)}{\sqrt{9\beta^2 + \left(1 - \beta^2\right)\left(1 - t\right)^2}} - \frac{\left(1 - \beta^2\right)t}{\sqrt{4\beta^2 + \left(1 - \beta^2\right)t^2}} \leq 0$$

So, $F(t) \leq F(0) = \sqrt{1 + 8\beta^2} - 2|\beta| \leq 1$ by taking $u = |\beta|$ in Remark 8. For $1 \leq t \leq 2$, we have

$$\begin{aligned}
0 &\geq -5t^2 - 8t + 4 \\
&= 4t^2 - 8t + 4 - 9t^2 \\
&= 4\left(t - 1\right)^2 - 9t^2.
\end{aligned}$$

Thus,

$$
\begin{aligned}
0 &\geq 4\beta^2 (t-1)^2 - 9\beta^2 t^2 \\
&= 4\beta^2 (t-1)^2 + (1-\beta^2) t^2 (t-1)^2 - \left(9\beta^2 t^2 + (1-\beta^2) t^2 (t-1)^2\right) \\
&= (t-1)^2 \left(4\beta^2 + (1-\beta^2) t^2\right) - t^2 \left(9\beta^2 + (1-\beta^2)(t-1)^2\right).
\end{aligned}
$$

Thus, by dividing by $\left(4\beta^2 + (1-\beta^2) t^2\right)\left(9\beta^2 + (1-\beta^2)(t-1)^2\right)$,we get

$$
\begin{aligned}
0 &\geq \frac{(t-1)^2}{\left(9\beta^2 + (1-\beta^2)(t-1)^2\right)} - \frac{t^2}{\left(4\beta^2 + (1-\beta^2) t^2\right)} \\
&= \left(\frac{(t-1)}{\sqrt{9\beta^2 + (1-\beta^2)(t-1)^2}} - \frac{t}{\sqrt{4\beta^2 + (1-\beta^2) t^2}}\right).
\end{aligned}
$$

Thus,

$$
F'(t) = \frac{(1-\beta^2)(t-1)}{\sqrt{9\beta^2 + (1-\beta^2)(t-1)^2}} - \frac{(1-\beta^2) t}{\sqrt{4\beta^2 + (1-\beta^2) t^2}} \leq 0,
$$

and $F(t) \leq F(1) = \sqrt{9\beta^2} - \sqrt{4\beta^2} = |\beta| \leq 1$.

Then, we get

$$
\begin{aligned}
\omega_3^2 - \lambda_- &= \frac{2 - \sqrt{4\beta^2 + (1-\beta^2)|z|^2}}{1-\beta^2} - \frac{3 - \sqrt{9\beta^2 + (1-\beta^2)|d|^2}}{1-\beta^2} \\
&= \frac{\sqrt{9\beta^2 + (1-\beta^2)|d|^2} - \sqrt{4\beta^2 + (1-\beta^2)|z|^2} - 1}{1-\beta^2} \\
&\leq 0.
\end{aligned}
$$

We have used Remark 9 in the last step. Thus, $\omega_3^2 < \lambda_-$ and $\omega_3^2 \notin [\lambda_-, \lambda_+]$. Similarly, we can show $\omega_4^2 > \lambda_+$ and $\omega_4^2 \notin [\lambda_-, \lambda_+]$. Figure 3.3 shows that $\omega_1^2\left(k_{||}\right)$ and $\omega_2^2\left(k_{||}\right)$ are located in the band gap $\left(\lambda_-\left(k_{||}\right), \lambda_+\left(k_{||}\right)\right)$ when $a = 1$ and $\beta = 0.1$.

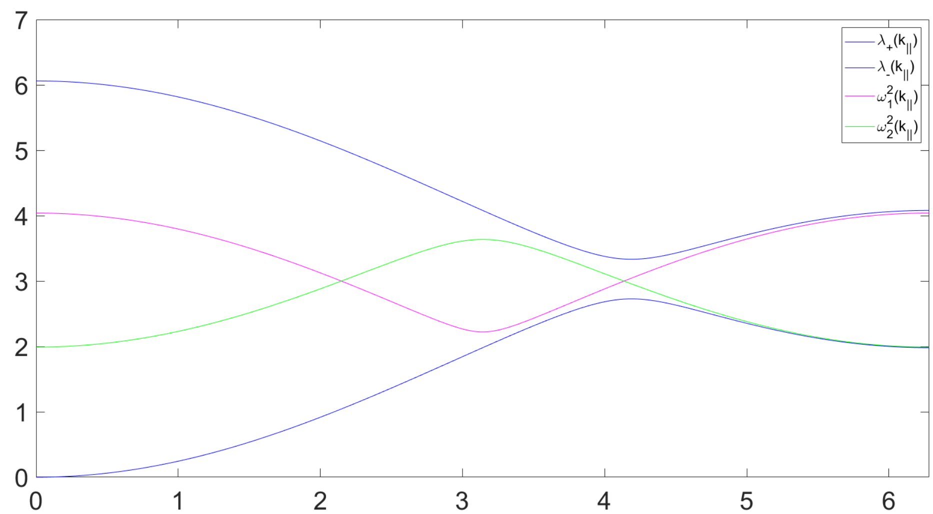

Figure 3.3: The upper and lower bands $\lambda_\pm\left(k_{||}\right)$, and the eigenvalues of the edge modes, $\omega_1^2\left(k_{||}\right)$ and $\omega_2^2\left(k_{||}\right)$, when $a = 1$ and $\beta = 0.1$.

Chapter 4

Gyroscopic Mechanical System

We consider the system obtained by replacing masses with identical gyroscopes hung to a plate in a two-dimensional mechanical system as in Figure C.1. We will use the same lattice vectors $\mathbf{a}_1$ and $\mathbf{a}_2$ as in Chapter 3 except taking $a = 1$ for simplicity.

The tips of gyroscopes will move under the effect of internal torque, $\mathbf{l}_m(t) \times m\mathbf{a}$, and external torque, $\mathbf{l}(t) \times \mathbf{F}$, where $\mathbf{l}(t) = \begin{bmatrix} x(t) \\ y(t) \\ -l \end{bmatrix}$ is the position of the tip of a gyroscope, $\mathbf{F} = \begin{bmatrix} F_1 \\ F_2 \\ 0 \end{bmatrix}$ is the force applied by the springs attached to the tip, $\mathbf{l}_m(t) = \frac{l_m}{l} \begin{bmatrix} x(t) \\ y(t) \\ -l \end{bmatrix}$ is the position of the center of mass of a gyroscope and $\mathbf{a} = \begin{bmatrix} 0 \\ 0 \\ -g \end{bmatrix}$ is the gravitational acceleration. Here l is the distance between the tip and the hanging point and l_m is the distance between the center of mass of a gyroscope and the hanging point of it. The behavior of a gyroscope under these effects is formulated as

$$\frac{I\Omega}{l}\frac{d\mathbf{l}(t)}{dt} = \mathbf{l}_m(t) \times m\mathbf{a} + \mathbf{l}(t) \times \mathbf{F}, \tag{4.1}$$

where I is the moment of inertia of a gyroscope, Ω is the angular speed of a gyroscope and m is the mass of the gyroscope. (4.1) can be simplified as

$$\begin{bmatrix} x' \\ y' \end{bmatrix} = \tau \begin{bmatrix} 0 & -1 \\ 1 & 0 \end{bmatrix} \begin{bmatrix} x \\ y \end{bmatrix} + \frac{\sigma}{k} \begin{bmatrix} 0 & 1 \\ -1 & 0 \end{bmatrix} \begin{bmatrix} F_1 \\ F_2 \end{bmatrix} \tag{4.2}$$

where $\tau = \frac{l_m mg}{I\Omega}$, $\sigma = \frac{l^2 k}{I\Omega}$ and k is the spring constant. Here, since the change of the position of the tip in the vertical direction is negligible, the third components of vectors are ignored.

4.1 Periodic Gyroscopic system

Over the periodic cell, by (4.2), the in-plane displacements $\mathbf{U}^a_{p,q}(t)$ and $\mathbf{U}^b_{p,q}(t)$ of the tip of gyroscopes a and b from their equilibrium position satisfy

$$\begin{aligned} \left(\mathbf{U}^a_{p,q}\right)' &= \begin{bmatrix} 0 & -\tau \\ \tau & 0 \end{bmatrix} \mathbf{U}^a_{p,q} + \begin{bmatrix} 0 & \sigma/k \\ -\sigma/k & 0 \end{bmatrix} \mathbf{F}^a_{p,q}, \\ \left(\mathbf{U}^b_{p,q}\right)' &= \begin{bmatrix} 0 & -\tau \\ \tau & 0 \end{bmatrix} \mathbf{U}^b_{p,q} + \begin{bmatrix} 0 & \sigma/k \\ -\sigma/k & 0 \end{bmatrix} \mathbf{F}^b_{p,q}, \end{aligned} \tag{4.3}$$

where $\mathbf{F}^a_{p,q}$ and $\mathbf{F}^b_{p,q}$ are the linearized spring forces applied by the springs and evaluated as

$$\begin{aligned} \mathbf{F}^a_{p,q} &= (-k)\left(M_1\left(\mathbf{U}^a_{p,q} - \mathbf{U}^b_{p,q}\right) + M_2\left(\mathbf{U}^a_{p,q} - \mathbf{U}^b_{p-1,q}\right) + M_3\left(\mathbf{U}^a_{p,q} - \mathbf{U}^b_{p,q-1}\right)\right) \\ \mathbf{F}^b_{p,q} &= (-k)\left(M_4\left(\mathbf{U}^b_{p,q} - \mathbf{U}^a_{p,q}\right) + M_5\left(\mathbf{U}^b_{p,q} - \mathbf{U}^a_{p,q+1}\right) M_6\left(\mathbf{U}^b_{p,q} - \mathbf{U}^a_{p+1,q}\right)\right) \end{aligned}$$

with

$$M_1 = M_4 = \frac{1}{4}\begin{bmatrix} 3 & \sqrt{3} \\ \sqrt{3} & 1 \end{bmatrix}, \; M_2 = M_6 = \frac{1}{4}\begin{bmatrix} 3 & -\sqrt{3} \\ -\sqrt{3} & 1 \end{bmatrix} \text{ and } M_3 = M_5 = \frac{1}{4}\begin{bmatrix} 0 & 0 \\ 0 & 4 \end{bmatrix}$$

Consider the time-harmonic solution in the form of

$$\mathbf{U}^a_{p,q}(t) = \begin{bmatrix} x_a \\ y_a \end{bmatrix} \exp\left[i(\omega t + \boldsymbol{\kappa}\cdot\mathbf{r}_{p,q})\right] \text{ and } \mathbf{U}^b_{p,q}(t) = \begin{bmatrix} x_b \\ y_b \end{bmatrix} \exp\left[i(\omega t + \boldsymbol{\kappa}\cdot\mathbf{r}_{p,q})\right], \quad (4.4)$$

where x_a, x_b, y_a and y_b are the amplitudes of the displacement of the tip of gyroscopes a and b along the x-axis and y-axis respectively and $\boldsymbol{\kappa}$ and $\mathbf{r}_{p,q}$ are as in Chapter 3. Then the amplitude vectors $\mathbf{u}_a = \begin{bmatrix} x_a \\ y_a \end{bmatrix}$ and $\mathbf{u}_b = \begin{bmatrix} x_b \\ y_b \end{bmatrix}$ satisfy

$$\begin{aligned}
i\omega\mathbf{u}_a = {} & \begin{bmatrix} 0 & -\tau \\ \tau & 0 \end{bmatrix} \mathbf{u}_a \\
& + \begin{bmatrix} 0 & -\sigma \\ \sigma & 0 \end{bmatrix} \left(\begin{bmatrix} \frac{3}{2} & 0 \\ 0 & \frac{3}{2} \end{bmatrix} \mathbf{u}_a - \frac{1}{4} \left(\begin{bmatrix} 3 & \sqrt{3} \\ \sqrt{3} & 1 \end{bmatrix} + \bar{e}_1 \begin{bmatrix} 3 & -\sqrt{3} \\ -\sqrt{3} & 1 \end{bmatrix} + \bar{e}_2 \begin{bmatrix} 0 & 0 \\ 0 & 4 \end{bmatrix} \right) \mathbf{u}_b \right) \\
i\omega\mathbf{u}_b = {} & \begin{bmatrix} 0 & -\tau \\ \tau & 0 \end{bmatrix} \mathbf{u}_b \\
& + \begin{bmatrix} 0 & -\sigma \\ \sigma & 0 \end{bmatrix} \left(\begin{bmatrix} \frac{3}{2} & 0 \\ 0 & \frac{3}{2} \end{bmatrix} \mathbf{u}_b - \frac{1}{4} \left(\begin{bmatrix} 3 & \sqrt{3} \\ \sqrt{3} & 1 \end{bmatrix} + e_1 \begin{bmatrix} 3 & -\sqrt{3} \\ -\sqrt{3} & 1 \end{bmatrix} + e_2 \begin{bmatrix} 0 & 0 \\ 0 & 4 \end{bmatrix} \right) \mathbf{u}_a \right)
\end{aligned}$$

where $e_1 = \exp(i\boldsymbol{\kappa}\cdot\mathbf{a}_1)$, $e_2 = \exp(i\boldsymbol{\kappa}\cdot\mathbf{a}_2)$ and $\bar{e}_1$ and $\bar{e}_2$ are complex conjugates. Then we have

$$\begin{aligned}
i\omega\mathbf{u}_a &= \begin{bmatrix} 0 & -\tau \\ \tau & 0 \end{bmatrix} \mathbf{u}_a + \begin{bmatrix} 0 & -\sigma \\ \sigma & 0 \end{bmatrix} \left(\begin{bmatrix} \frac{3}{2} & 0 \\ 0 & \frac{3}{2} \end{bmatrix} \mathbf{u}_a - \frac{1}{4} \begin{bmatrix} 3(1+\bar{e}_1) & \sqrt{3}(1-\bar{e}_1) \\ \sqrt{3}(1-\bar{e}_1) & 1+\bar{e}_1+4\bar{e}_2 \end{bmatrix} \mathbf{u}_b \right) \\
i\omega\mathbf{u}_b &= \begin{bmatrix} 0 & -\tau \\ \tau & 0 \end{bmatrix} \mathbf{u}_b + \begin{bmatrix} 0 & -\sigma \\ \sigma & 0 \end{bmatrix} \left(\begin{bmatrix} \frac{3}{2} & 0 \\ 0 & \frac{3}{2} \end{bmatrix} \mathbf{u}_b - \frac{1}{4} \begin{bmatrix} 3(1+\bar{e}_1) & \sqrt{3}(1-\bar{e}_1) \\ \sqrt{3}(1-\bar{e}_1) & 1+\bar{e}_1+4\bar{e}_2 \end{bmatrix} \mathbf{u}_a \right),
\end{aligned}$$

which is equivalent to

$$
\begin{aligned}
i\omega \mathbf{u}_a &= \begin{bmatrix} 0 & -\left(\tau + \frac{3\sigma}{2}\right) \\ \tau + \frac{3\sigma}{2} & 0 \end{bmatrix} \mathbf{u}_a + \begin{bmatrix} \frac{\sigma\sqrt{3}}{4}\left(1-\overline{e}_1\right) & \frac{\sigma}{4}\left(1+\overline{e}_1+4\overline{e}_2\right) \\ -\frac{3\sigma}{4}\left(\overline{e}_1+1\right) & \frac{\sigma\sqrt{3}}{4}\left(\overline{e}_1-1\right) \end{bmatrix} \mathbf{u}_b \\
i\omega \mathbf{u}_b &= \begin{bmatrix} \frac{\sigma\sqrt{3}}{4}\left(1-e_1\right) & \frac{\sigma}{4}\left(1+e_1+4e_2\right) \\ -\frac{3\sigma}{4}\left(e_1+1\right) & \frac{\sigma\sqrt{3}}{4}\left(e_1-1\right) \end{bmatrix} \mathbf{u}_a + \begin{bmatrix} 0 & -\left(\tau + \frac{3\sigma}{2}\right) \\ \tau + \frac{3\sigma}{2} & 0 \end{bmatrix} \mathbf{u}_b .
\end{aligned}
\tag{4.5}
$$

For $\mathbf{u} = \begin{bmatrix} \mathbf{u}_a \\ \mathbf{u}_b \end{bmatrix}$, (4.5) can be written as

$$
i\omega \mathbf{u} = \begin{bmatrix} 0 & -\left(\tau + \frac{3\sigma}{2}\right) & \frac{\sigma\sqrt{3}}{4}\left(1-\overline{e}_1\right) & \frac{\sigma}{4}\left(1+\overline{e}_1+4\overline{e}_2\right) \\ \tau + \frac{3\sigma}{2} & 0 & -\frac{3\sigma}{4}\left(\overline{e}_1+1\right) & \frac{\sigma\sqrt{3}}{4}\left(\overline{e}_1-1\right) \\ \frac{\sigma\sqrt{3}}{4}\left(1-e_1\right) & \frac{\sigma}{4}\left(1+e_1+4e_2\right) & 0 & -\left(\tau + \frac{3\sigma}{2}\right) \\ -\frac{3\sigma}{4}\left(e_1+1\right) & \frac{\sigma\sqrt{3}}{4}\left(e_1-1\right) & \tau + \frac{3\sigma}{2} & 0 \end{bmatrix} \mathbf{u} \tag{4.6}
$$

The topological invariant we use to characterize the bulk of the spring-gyroscope system is the Chern number. In Chapter 3, the valley Chern number which describes the topology localized near valleys is used. In contrast, the Chern number characterizes the topology over the entire Brillouin zone and is defined as (**??**)

$$
C = \frac{1}{2\pi} \oint_{\partial \mathbb{B}} B(\boldsymbol{\kappa}) \cdot d\boldsymbol{\kappa} = \frac{1}{2\pi} \int_{\mathbb{B}} \Omega(\boldsymbol{\kappa}) d\boldsymbol{\kappa}
$$

where $B(\boldsymbol{\kappa})$ and $\Omega(\boldsymbol{\kappa})$ are the Berry connection and the Berry curvature, respectively, as defined in Chapter 3 and $\mathbb{B}$ is the Brillouin zone.

By the numerical evaluation, the band structure of the system in (4.6) and the Chern numbers are evaluated for $g > 0$ and $g < 0$. Figure 4.1 provides two of the bands. The other two bands have the opposite sign of these bands. An identical band structure can be obtained for suitable choices of $g < 0$. However, when $g > 0$, the Chern number of the system is 1, but it is -1 when $g < 0$.

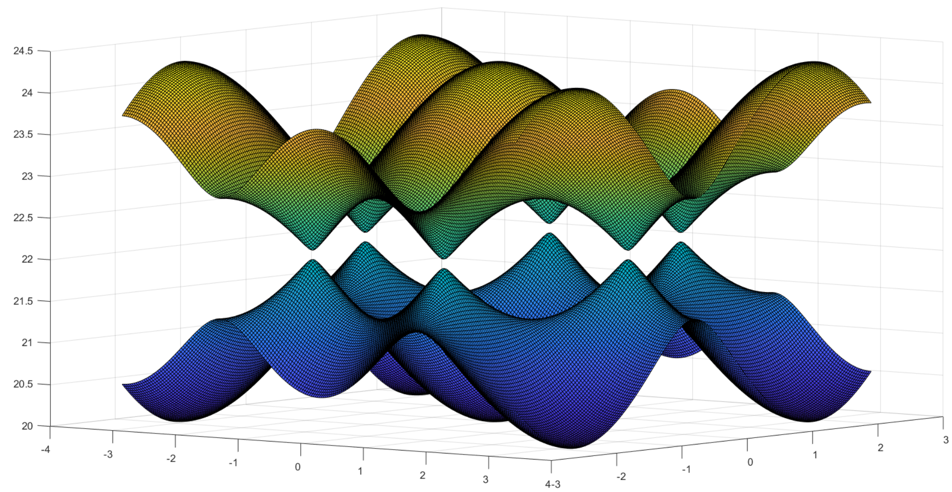

Figure 4.1: The bands above xy-plane of the band structure of the gyroscopic system when $g = 20$. Other two bands are symmetric to these with respect to xy-plane. When a suitable choice of $g < 0$ is made, the band structure is the same.

4.2 Edge Modes for the Gyroscopic Mechanical System

We consider a joint system formed by gluing two periodic hexagonal lattices with $g < 0$ and $g > 0$. For the $g < 0$ case, we use g_l instead of $g < 0$. As in Chapter 3, the interface is parallel to $\mathbf{a}_2$ with $g < 0$ for gyroscope b but $g > 0$ for gyroscope a as in Figure C.2. From Section 4.1, two sides of the interface have different Chern numbers, -1 and 1.

4.2.1 Transfer Matrices

For $p \in \mathbb{Z}^+$ and $q \in \mathbb{Z}$, the governing equations of the gyroscopes located at the left and the right sides of the interface are

$$
\begin{aligned}
\left(\mathbf{U}^a_{-p,q}\right)' &= \begin{bmatrix} 0 & -\tau_l \\ \tau_l & 0 \end{bmatrix} \mathbf{U}^a_{-p,q} + \begin{bmatrix} 0 & \frac{\sigma}{k} \\ -\frac{\sigma}{k} & 0 \end{bmatrix} \mathbf{F}^a_{-p,q}, \\
\left(\mathbf{U}^b_{-(p+1),q}\right)' &= \begin{bmatrix} 0 & -\tau_l \\ \tau_l & 0 \end{bmatrix} \mathbf{U}^b_{-(p+1),q} + \begin{bmatrix} 0 & \frac{\sigma}{k} \\ -\frac{\sigma}{k} & 0 \end{bmatrix} \mathbf{F}^b_{-(p+1),q},
\end{aligned}
\tag{4.7}
$$

where, $\tau_l = \frac{l_m m g_l}{I\Omega}$ and

$$
\begin{aligned}
\mathbf{F}^a_{-p,q} = (-k)\Big(& M_1\left(\mathbf{U}^a_{-p,q} - \mathbf{U}^b_{-p,q}\right) \\
& + M_2\left(\mathbf{U}^a_{-p,q} - \mathbf{U}^b_{-(p+1),q}\right) \\
& + M_3\left(\mathbf{U}^a_{-p,q} - \mathbf{U}^b_{-p,q+1}\right)\Big), \\
\mathbf{F}^b_{-(p+1),q} = (-k)\Big(& M_4\left(\mathbf{U}^b_{-(p+1),q} - \mathbf{U}^a_{-(p+1),q}\right) \\
& + M_5\left(\mathbf{U}^b_{-(p+1),q} - \mathbf{U}^a_{-(p+1),q+1}\right) \\
& + M_6\left(\mathbf{U}^b_{-(p+1),q} - \mathbf{U}^a_{-p,q}\right)\Big),
\end{aligned}
$$

and

$$
\begin{aligned}
\left(\mathbf{U}^a_{p+1,q}\right)' &= \begin{bmatrix} 0 & -\tau \\ \tau & 0 \end{bmatrix} \mathbf{U}^a_{p+1,q} + \begin{bmatrix} 0 & \frac{\sigma}{k} \\ -\frac{\sigma}{k} & 0 \end{bmatrix} \mathbf{F}^a_{p+1,q}, \\
\left(\mathbf{U}^b_{p,q}\right)' &= \begin{bmatrix} 0 & -\tau \\ \tau & 0 \end{bmatrix} \mathbf{U}^b_{p,q} + \begin{bmatrix} 0 & \frac{\sigma}{k} \\ -\frac{\sigma}{k} & 0 \end{bmatrix} \mathbf{F}^b_{p,q},
\end{aligned}
\tag{4.8}
$$

where

$$\mathbf{F}^a_{p+1,q} = (-k)\left(M_1\left(\mathbf{U}^a_{p+1,q} - \mathbf{U}^b_{p+1,q}\right) + M_2\left(\mathbf{U}^a_{p+1,q} - \mathbf{U}^b_{p,q}\right) + M_3\left(\mathbf{U}^a_{p+1,q} - \mathbf{U}^b_{p+1,q-1}\right)\right),$$
$$\mathbf{F}^b_{p,q} = (-k)\left(M_4\left(\mathbf{U}^b_{p,q} - \mathbf{U}^a_{p,q}\right) + M_5\left(\mathbf{U}^b_{p,q} - \mathbf{U}^a_{p,q+1}\right) + M_6\left(\mathbf{U}^b_{p,q} - \mathbf{U}^a_{p+1,q}\right)\right)$$

respectively. The governing equation for the gyroscopes located at the interface are

$$\begin{aligned}\left(\mathbf{U}^a_{1,q}\right)' &= \begin{bmatrix} 0 & -\tau \\ \tau & 0 \end{bmatrix} \mathbf{U}^a_{1,q} + \begin{bmatrix} 0 & \frac{\sigma}{k} \\ -\frac{\sigma}{k} & 0 \end{bmatrix} \mathbf{F}^a_{1,q}, \\ \left(\mathbf{U}^b_{-1,q}\right)' &= \begin{bmatrix} 0 & -\tau_l \\ \tau_l & 0 \end{bmatrix} \mathbf{U}^b_{-1,q} + \begin{bmatrix} 0 & \frac{\sigma}{k} \\ -\frac{\sigma}{k} & 0 \end{bmatrix} \mathbf{F}^b_{-1,q},\end{aligned} \tag{4.9}$$

where

$$\mathbf{F}^a_{1,q} = (-k)\left(M_1\left(\mathbf{U}^a_{1,q} - \mathbf{U}^b_{1,q}\right) + M_2\left(\mathbf{U}^a_{1,q} - \mathbf{U}^b_{-1,q}\right) + M_3\left(\mathbf{U}^a_{1,q} - \mathbf{U}^b_{1,q-1}\right)\right)$$
$$\mathbf{F}^b_{-1,q} = (-k)\left(M_4\left(\mathbf{U}^b_{-1,q} - \mathbf{U}^a_{-1,q}\right) + M_5\left(\mathbf{U}^b_{-1,q} - \mathbf{U}^a_{-1,q+1}\right) + M_6\left(\mathbf{U}^b_{-1,q} - \mathbf{U}^a_{1,q}\right)\right).$$

For each $k_{||} \in [0, 2\pi]$, we consider the solutions that propagate along the interface and decay along the horizontal direction by letting

$$\mathbf{U}^a_{p,q}(t) = \begin{bmatrix} x_a \\ y_a \end{bmatrix}_p e^{i\left(\omega t + k_{||} q\right)} \text{ and } \mathbf{U}^b_{p,q}(t) = \begin{bmatrix} x_b \\ y_b \end{bmatrix}_p e^{i\left(\omega t + k_{||} q\right)}. \tag{4.10}$$

An edge mode $\left(\mathbf{U}^a_{p,q}(t), \mathbf{U}^b_{p,q}(t)\right)$ is the nontrivial solution to (4.7) - (4.9) which decays to zero as $p \to \infty$.

We aim to show numerically the existence of an edge mode for the joint system in Figure C.2 when g has opposite signs on each side of the interface. For $k_{||} \in [0, 2\pi]$, the eigenfrequency $\omega(k_{||})$ will be in the common band gap $\left(\lambda_-\left(k_{||}\right), \lambda_+\left(k_{||}\right)\right)$. Note that the definitions of $\lambda_\pm\left(k_{||}\right)$ are as in (3.21), but the bands are evaluated for the gyroscopic mechanical system.

For (4.7) - (4.9), we consider the solutions of the form (4.10). In the right gyroscopic system, by (4.8), $\mathbf{u}_p^a = \begin{bmatrix} x_a \\ y_a \end{bmatrix}_p$ and $\mathbf{u}_p^b = \begin{bmatrix} x_b \\ y_b \end{bmatrix}_p$ satisfy

$$\begin{aligned}
i\omega\mathbf{u}_{p+1}^a &= \begin{bmatrix} 0 & -\tau \\ \tau & 0 \end{bmatrix} \mathbf{u}_{p+1}^a \\
&\quad + \begin{bmatrix} 0 & -\sigma \\ \sigma & 0 \end{bmatrix} \left(\begin{bmatrix} \frac{3}{2} & 0 \\ 0 & \frac{3}{2} \end{bmatrix} \mathbf{u}_{p+1}^a - \begin{bmatrix} \frac{3}{4} & \frac{\sqrt{3}}{4} \\ \frac{\sqrt{3}}{4} & \frac{1+4\bar{e}}{4} \end{bmatrix} \mathbf{u}_{p+1}^b - \begin{bmatrix} \frac{3}{4} & -\frac{\sqrt{3}}{4} \\ -\frac{\sqrt{3}}{4} & \frac{1}{4} \end{bmatrix} \mathbf{u}_p^b \right) \\
i\omega\mathbf{u}_p^b &= \begin{bmatrix} 0 & -\tau \\ \tau & 0 \end{bmatrix} \mathbf{u}_p^b \\
&\quad + \begin{bmatrix} 0 & -\sigma \\ \sigma & 0 \end{bmatrix} \left(\begin{bmatrix} \frac{3}{2} & 0 \\ 0 & \frac{3}{2} \end{bmatrix} \mathbf{u}_p^b - \begin{bmatrix} \frac{3}{4} & \frac{\sqrt{3}}{4} \\ \frac{\sqrt{3}}{4} & \frac{1+4\bar{e}}{4} \end{bmatrix} \mathbf{u}_p^a - \begin{bmatrix} \frac{3}{4} & -\frac{\sqrt{3}}{4} \\ -\frac{\sqrt{3}}{4} & \frac{1}{4} \end{bmatrix} \mathbf{u}_{p+1}^a \right)
\end{aligned} \tag{4.11}$$

where $e = e^{ik_\parallel}$. (4.11) can be simplified as

$$\begin{aligned}
\begin{bmatrix} -\sqrt{3} & -(1+4e) \\ 3 & \sqrt{3} \end{bmatrix} \mathbf{u}_p^a + \begin{bmatrix} \frac{4i\omega}{\sigma} & \frac{4}{\sigma}\left(\tau + \frac{3\sigma}{2}\right) \\ -\frac{4}{\sigma}\left(\tau + \frac{3\sigma}{2}\right) & \frac{4i\omega}{\sigma} \end{bmatrix} \mathbf{u}_p^b &= \begin{bmatrix} -\sqrt{3} & 1 \\ -3 & \sqrt{3} \end{bmatrix} \mathbf{u}_{p+1}^a, \\
\begin{bmatrix} \sqrt{3} & -1 \\ 3 & -\sqrt{3} \end{bmatrix} \mathbf{u}_p^b = \begin{bmatrix} -\frac{4i\omega}{\sigma} & -\frac{4}{\sigma}\left(\tau + \frac{3\sigma}{2}\right) \\ \frac{4}{\sigma}\left(\tau + \frac{3\sigma}{2}\right) & -\frac{4i\omega}{\sigma} \end{bmatrix} \mathbf{u}_{p+1}^a &+ \begin{bmatrix} \sqrt{3} & 1+4\bar{e} \\ -3 & -\sqrt{3} \end{bmatrix} \mathbf{u}_{p+1}^b.
\end{aligned}$$

It reduces to

$$R_1\mathbf{u}_p = R_2\mathbf{u}_{p+1} \tag{4.12}$$

where

$$R_1 = \begin{bmatrix} -\sqrt{3} & -(1+4e) & \frac{4i\omega}{\sigma} & \frac{4}{\sigma}\left(\tau+\frac{3\sigma}{2}\right) \\ 3 & \sqrt{3} & -\frac{4}{\sigma}\left(\tau+\frac{3\sigma}{2}\right) & \frac{4i\omega}{\sigma} \\ 0 & 0 & \sqrt{3} & -1 \\ 0 & 0 & 3 & -\sqrt{3} \end{bmatrix}$$

and

$$R_2 = \begin{bmatrix} -\sqrt{3} & 1 & 0 & 0 \\ -3 & \sqrt{3} & 0 & 0 \\ -\frac{4i\omega}{\sigma} & -\frac{4}{\sigma}\left(\tau+\frac{3\sigma}{2}\right) & \sqrt{3} & 1+4\bar{e} \\ \frac{4}{\sigma}\left(\tau+\frac{3\sigma}{2}\right) & -\frac{4i\omega}{\sigma} & -3 & -\sqrt{3} \end{bmatrix}.$$

Similarly, in the left gyroscopic system, by (4.7), $\mathbf{u}^a_{-p} = \begin{bmatrix} x_a \\ y_a \end{bmatrix}_{-p}$ and $\mathbf{u}^b_{-p} = \begin{bmatrix} x_b \\ y_b \end{bmatrix}_{-p}$ satisfy

$$\begin{aligned} i\omega\mathbf{u}^a_{-p} &= \begin{bmatrix} 0 & -\tau_l \\ \tau_l & 0 \end{bmatrix} \mathbf{u}^a_{-p} \\ &\quad + \begin{bmatrix} 0 & -\sigma \\ \sigma & 0 \end{bmatrix} \left(\begin{bmatrix} \frac{3}{2} & 0 \\ 0 & \frac{3}{2} \end{bmatrix} \mathbf{u}^a_{-p} - \begin{bmatrix} \frac{3}{4} & \frac{\sqrt{3}}{4} \\ \frac{\sqrt{3}}{4} & \frac{1+4\bar{e}}{4} \end{bmatrix} \mathbf{u}^b_{-p} - \begin{bmatrix} \frac{3}{4} & -\frac{\sqrt{3}}{4} \\ -\frac{\sqrt{3}}{4} & \frac{1}{4} \end{bmatrix} \mathbf{u}^b_{-(p+1)} \right) \\ i\omega\mathbf{u}^b_{-(p+1)} &= \begin{bmatrix} 0 & -\tau_l \\ \tau_l & 0 \end{bmatrix} \mathbf{u}^b_{-(p+1)} \\ &\quad + \begin{bmatrix} 0 & -\sigma \\ \sigma & 0 \end{bmatrix} \left(\begin{bmatrix} \frac{3}{2} & 0 \\ 0 & \frac{3}{2} \end{bmatrix} \mathbf{u}^b_{-(p+1)} - \begin{bmatrix} \frac{3}{4} & \frac{\sqrt{3}}{4} \\ \frac{\sqrt{3}}{4} & \frac{1+4e}{4} \end{bmatrix} \mathbf{u}^a_{-(p+1)} - \begin{bmatrix} \frac{3}{4} & -\frac{\sqrt{3}}{4} \\ -\frac{\sqrt{3}}{4} & \frac{1}{4} \end{bmatrix} \mathbf{u}^a_{-p} \right), \end{aligned} \tag{4.13}$$

where $\tau_l = \frac{l_m m g_l}{I\Omega}$. (4.13) is simplified as

$$\begin{bmatrix} \frac{4i\omega}{\sigma} & \frac{4}{\sigma}\left(\tau_l + \frac{3\sigma}{2}\right) \\ -\frac{4}{\sigma}\left(\tau_l + \frac{3\sigma}{2}\right) & \frac{4i\omega}{\sigma} \end{bmatrix} \mathbf{u}^a_{-p} + \begin{bmatrix} -\sqrt{3} & -(1+4\bar{e}) \\ 3 & \sqrt{3} \end{bmatrix} \mathbf{u}^b_{-p} = \begin{bmatrix} -\sqrt{3} & 1 \\ -3 & \sqrt{3} \end{bmatrix} \mathbf{u}^b_{-(p+1)}$$

$$\begin{bmatrix} \sqrt{3} & -1 \\ 3 & -\sqrt{3} \end{bmatrix} \mathbf{u}^a_{-p} = \begin{bmatrix} \sqrt{3} & 1+4e \\ -3 & -\sqrt{3} \end{bmatrix} \mathbf{u}^a_{-(p+1)} + \begin{bmatrix} -\frac{4i\omega}{\sigma} & -\frac{4}{\sigma}\left(\tau_l + \frac{3\sigma}{2}\right) \\ \frac{4}{\sigma}\left(\tau_l + \frac{3\sigma}{2}\right) & -\frac{4i\omega}{\sigma} \end{bmatrix} \mathbf{u}^b_{-(p+1)}.$$

It reduces to

$$L_1 \mathbf{u}_{-p} = L_2 \mathbf{u}_{-(p+1)} \tag{4.14}$$

where

$$L_1 = \begin{bmatrix} \frac{4i\omega}{\sigma} & \frac{4}{\sigma}\left(\tau_l + \frac{3\sigma}{2}\right) & -\sqrt{3} & -(1+4\bar{e}) \\ -\frac{4}{\sigma}\left(\tau_l + \frac{3\sigma}{2}\right) & \frac{4i\omega}{\sigma} & 3 & \sqrt{3} \\ \sqrt{3} & -1 & 0 & 0 \\ 3 & -\sqrt{3} & 0 & 0 \end{bmatrix}$$

and

$$L_2 = \begin{bmatrix} 0 & 0 & -\sqrt{3} & 1 \\ 0 & 0 & -3 & \sqrt{3} \\ \sqrt{3} & 1+4e & -\frac{4i\omega}{\sigma} & -\frac{4}{\sigma}\left(\tau_l + \frac{3\sigma}{2}\right) \\ -3 & -\sqrt{3} & \frac{4}{\sigma}\left(\tau_l + \frac{3\sigma}{2}\right) & -\frac{4i\omega}{\sigma} \end{bmatrix}.$$

Since all matrices are singular, there is no single matrix that relates two horizontally consecutive cells on either side of the interface. Thus, the relations are obtained by (4.12) and (4.14) for the left and right sides of the interface respectively. For the gyroscopes at the interface of the joint system, by (4.9) and (4.10), we obtain

$$
\begin{aligned}
i\omega \mathbf{u}_1^a &= \begin{bmatrix} 0 & -\tau \\ \tau & 0 \end{bmatrix} \mathbf{u}_1^a + \begin{bmatrix} 0 & -\sigma \\ \sigma & 0 \end{bmatrix} \left(\begin{bmatrix} \frac{3}{2} & 0 \\ 0 & \frac{3}{2} \end{bmatrix} \mathbf{u}_1^a - \begin{bmatrix} \frac{3}{4} & \frac{\sqrt{3}}{4} \\ \frac{\sqrt{3}}{4} & \frac{1+4\bar{e}}{4} \end{bmatrix} \mathbf{u}_1^b - \begin{bmatrix} \frac{3}{4} & -\frac{\sqrt{3}}{4} \\ -\frac{\sqrt{3}}{4} & \frac{1}{4} \end{bmatrix} \mathbf{u}_{-1}^b \right), \\
i\omega \mathbf{u}_{-1}^b &= \begin{bmatrix} 0 & -\tau_l \\ \tau_l & 0 \end{bmatrix} \mathbf{u}_{-1}^b + \begin{bmatrix} 0 & -\sigma \\ \sigma & 0 \end{bmatrix} \left(\begin{bmatrix} \frac{3}{2} & 0 \\ 0 & \frac{3}{2} \end{bmatrix} \mathbf{u}_{-1}^b - \begin{bmatrix} \frac{3}{4} & \frac{\sqrt{3}}{4} \\ \frac{\sqrt{3}}{4} & \frac{1+4e}{4} \end{bmatrix} \mathbf{u}_{-1}^a - \begin{bmatrix} \frac{3}{4} & -\frac{\sqrt{3}}{4} \\ -\frac{\sqrt{3}}{4} & \frac{1}{4} \end{bmatrix} \mathbf{u}_1^a \right).
\end{aligned}
\tag{4.15}
$$

(4.15) is simplified as

$$
\begin{aligned}
\begin{bmatrix} \sqrt{3} & -1 \\ 3 & -\sqrt{3} \end{bmatrix} \mathbf{u}_{-1}^b &= \begin{bmatrix} \frac{4i\omega}{\sigma} & -\frac{4}{\sigma}\left(\tau + \frac{3\sigma}{2}\right) \\ \frac{4}{\sigma}\left(\tau + \frac{3\sigma}{2}\right) & \frac{4i\omega}{\sigma} \end{bmatrix} \mathbf{u}_1^a + \begin{bmatrix} \frac{\sqrt{3}}{4} & \frac{1+4\bar{e}}{4} \\ -\frac{3}{4} & -\frac{\sqrt{3}}{4} \end{bmatrix} \mathbf{u}_1^b, \\
\begin{bmatrix} -\frac{\sqrt{3}}{4} & -\frac{1+4e}{4} \\ \frac{3}{4} & \frac{\sqrt{3}}{4} \end{bmatrix} \mathbf{u}_{-1}^a + \begin{bmatrix} \frac{4i\omega}{\sigma} & \frac{4}{\sigma}\left(\tau_l + \frac{3\sigma}{2}\right) \\ -\frac{4}{\sigma}\left(\tau_l + \frac{3\sigma}{2}\right) & \frac{4i\omega}{\sigma} \end{bmatrix} \mathbf{u}_{-1}^b &= \begin{bmatrix} -\frac{\sqrt{3}}{4} & \frac{1}{4} \\ -\frac{3}{4} & \frac{\sqrt{3}}{4} \end{bmatrix} \mathbf{u}_1^a.
\end{aligned}
$$

It reduces to

$$
S_1 \mathbf{u}_{-1} = S_2 \mathbf{u}_1
$$

where

$$
S_1 = \begin{bmatrix} 0 & 0 & \sqrt{3} & -1 \\ 0 & 0 & 3 & -\sqrt{3} \\ -\frac{\sqrt{3}}{4} & -\frac{1+4e}{4} & \frac{4i\omega}{\sigma} & \frac{4}{\sigma}\left(\tau_l + \frac{3\sigma}{2}\right) \\ \frac{3}{4} & \frac{\sqrt{3}}{4} & -\frac{4}{\sigma}\left(\tau_l + \frac{3\sigma}{2}\right) & \frac{4i\omega}{\sigma} \end{bmatrix}
$$

and

$$S_2 = \begin{bmatrix} \frac{4i\omega}{\sigma} & -\frac{4}{\sigma}\left(\tau + \frac{3\sigma}{2}\right) & \frac{\sqrt{3}}{4} & \frac{1+4\bar{e}}{4} \\ \frac{4}{\sigma}\left(\tau + \frac{3\sigma}{2}\right) & \frac{4i\omega}{\sigma} & -\frac{3}{4} & -\frac{\sqrt{3}}{4} \\ -\frac{\sqrt{3}}{4} & \frac{1}{4} & 0 & 0 \\ -\frac{3}{4} & \frac{\sqrt{3}}{4} & 0 & 0 \end{bmatrix}$$

In this section, we derived the transfer matrices that describe the propagation of the solutions along both sides of the interface and matrices governing the solution at the interface. These matrices formulate the transfer matrix approach and characterize how the solution behaves along the lattice. They serve as a framework to understand the solution. In the next section, we study a finite system of equations for the gyroscopic mechanical system and mention our ongoing studies about how to relate these two approaches.

4.2.2 Finite system

In Section 4.1, we have the governing equations for two gyroscopes from two consecutive cells, p and $p+1$ on the right system and $-p$ and $-(p+1)$ on the left system, in the horizontal direction in order to obtain transfer relations between horizontally consecutive cells. If we write governing equations for the gyroscopes from the same cell, we obtain a system of equations that relates three horizontally consecutive cells, $p-1$, p and $p+1$ or $-(p+1)$, $-p$ and $-(p-1)$. When these equation systems are obtained for $p = 1, 2, ...$ and $p = -1, -2, ...$ we get an infinite system. In this part, our purpose is to truncate this infinite system in order to obtain a finite system that includes the governing equations from both sides of the interface and the interface itself by using the definition of edge modes. The frequency obtained from the truncated system is an approximation for the edge mode frequency of the original system.

For this purpose, for $p = 2, 3, ...$, we have

$$\left(\mathbf{U}_{p,q}^{a}\right)' = \begin{bmatrix} 0 & -\tau \\ \tau & 0 \end{bmatrix} \mathbf{U}_{p,q}^{a} + \begin{bmatrix} 0 & \sigma/k \\ -\sigma/k & 0 \end{bmatrix} \mathbf{F}_{p,q}^{a},$$
$$\left(\mathbf{U}_{p,q}^{b}\right)' = \begin{bmatrix} 0 & -\tau \\ \tau & 0 \end{bmatrix} \mathbf{U}_{p,q}^{b} + \begin{bmatrix} 0 & \sigma/k \\ -\sigma/k & 0 \end{bmatrix} \mathbf{F}_{p,q}^{b}, \tag{4.16}$$

where $\left(\mathbf{U}_{p,q}^{a}, \mathbf{U}_{p,q}^{b}\right)$ are in (4.10) and

$$\mathbf{F}_{p,q}^{a} = (-k)\left(M_1\left(\mathbf{u}_{p,q}^{a} - \mathbf{u}_{p,q}^{b}\right) + M_2\left(\mathbf{u}_{p,q}^{a} - \mathbf{u}_{p-1,q}^{b}\right) + M_3\left(\mathbf{u}_{p,q}^{a} - \mathbf{u}_{p,q-1}^{b}\right)\right),$$
$$\mathbf{F}_{p,q}^{b} = (-k)\left(M_4\left(\mathbf{u}_{p,q}^{b} - \mathbf{u}_{p,q}^{a}\right) + M_5\left(\mathbf{u}_{p,q}^{b} - \mathbf{u}_{p,q+1}^{a}\right) + M_6\left(\mathbf{u}_{p,q}^{b} - \mathbf{u}_{p+1,q}^{a}\right)\right) \tag{4.17}$$

which reduces (4.16) to

$$i\omega\mathbf{u}_{p}^{a} = \begin{bmatrix} 0 & -\left(\tau + \frac{3\sigma}{2}\right) \\ \left(\tau + \frac{3\sigma}{2}\right) & 0 \end{bmatrix} \mathbf{u}_{p}^{a} + \frac{\sigma}{4}\begin{bmatrix} \sqrt{3} & 1+4\overline{e} \\ -3 & -\sqrt{3} \end{bmatrix} \mathbf{u}_{p}^{b} + \frac{\sigma}{4}\begin{bmatrix} -\sqrt{3} & 1 \\ -3 & \sqrt{3} \end{bmatrix} \mathbf{u}_{p-1}^{b},$$
$$i\omega\mathbf{u}_{p}^{b} = \frac{\sigma}{4}\begin{bmatrix} \sqrt{3} & 1+4e \\ -3 & -\sqrt{3} \end{bmatrix} \mathbf{u}_{p}^{a} + \begin{bmatrix} 0 & -\left(\tau + \frac{3\sigma}{2}\right) \\ \left(\tau + \frac{3\sigma}{2}\right) & 0 \end{bmatrix} \mathbf{u}_{p}^{b} + \frac{\sigma}{4}\begin{bmatrix} -\sqrt{3} & 1 \\ -3 & \sqrt{3} \end{bmatrix} \mathbf{u}_{p+1}^{a}.$$

It can be written as

$$i\omega\mathbf{u}_{p}^{a} = C\mathbf{u}_{p-1}^{b} + A\mathbf{u}_{p}^{a} + \overline{B}\mathbf{u}_{p}^{b}$$
$$i\omega\mathbf{u}_{p}^{b} = B\mathbf{u}_{p}^{a} + A\mathbf{u}_{p}^{b} + C\mathbf{u}_{p+1}^{a} \tag{4.18}$$

where

$$A = \begin{bmatrix} 0 & -\left(\tau + \frac{3\sigma}{2}\right) \\ \left(\tau + \frac{3\sigma}{2}\right) & 0 \end{bmatrix}, B = \frac{\sigma}{4}\begin{bmatrix} \sqrt{3} & 1+4e \\ -3 & -\sqrt{3} \end{bmatrix} \text{ and } C = \frac{\sigma}{4}\begin{bmatrix} -\sqrt{3} & 1 \\ -3 & \sqrt{3} \end{bmatrix}.$$

By using block matrices, (4.18) can be written as

$$i\omega\mathbf{u}_{p} = P\mathbf{u}_{p-1} + Q\mathbf{u}_{p} + R\mathbf{u}_{p+1}$$

where

$$P = \begin{bmatrix} \mathbf{0}_{2\times 2} & C \\ \mathbf{0}_{2\times 2} & \mathbf{0}_{2\times 2} \end{bmatrix}, \; Q = \begin{bmatrix} A & \overline{B} \\ B & A \end{bmatrix} \text{ and } R = \begin{bmatrix} \mathbf{0}_{2\times 2} & \mathbf{0}_{2\times 2} \\ C & \mathbf{0}_{2\times 2} \end{bmatrix}$$

where $\mathbf{u}_p = \begin{bmatrix} \mathbf{u}_p^a \\ \mathbf{u}_p^b \end{bmatrix}$ and $\mathbf{0}_{2\times 2} = \begin{bmatrix} 0 & 0 \\ 0 & 0 \end{bmatrix}$. By switching p to $-p$ and τ to τ_l, we obtain the governing equations for the left side of the interface as

$$i\omega \mathbf{u}_{-p} = P\mathbf{u}_{-(p+1)} + Q_l \mathbf{u}_{-p} + R\mathbf{u}_{-(p-1)}$$

where

$$Q_l = \begin{bmatrix} A_l & \overline{B} \\ B & A_l \end{bmatrix} \text{ and } A_l = \begin{bmatrix} 0 & -\left(\tau_l + \frac{3\sigma}{2}\right) \\ \left(\tau_l + \frac{3\sigma}{2}\right) & 0 \end{bmatrix}$$

By similar calculations for the $p = -1$ and $p = 1$ cases, we obtain

$$i\omega \mathbf{u}_{-1} = P\mathbf{u}_{-2} + Q_l \mathbf{u}_{-1} + R\mathbf{u}_1,$$

and

$$i\omega \mathbf{u}_1 = P\mathbf{u}_{-1} + Q\mathbf{u}_1 + R\mathbf{u}_2.$$

Therefore, the governing equations can be written as an infinite dimensional system,

$$i\omega \mathbf{u} = H\mathbf{u} \tag{4.19}$$

where

$$\mathbf{u} = \begin{bmatrix} \vdots \\ \mathbf{u}_{-2} \\ \mathbf{u}_{-1} \\ \mathbf{u}_{1} \\ \mathbf{u}_{2} \\ \vdots \end{bmatrix}, \text{ and } H = \begin{bmatrix} \ddots & \ddots & & & & \\ \ddots & Q_l & R & & & \\ & P & Q_l & R & & \\ & & P & Q & R & \\ & & & P & Q & \ddots \\ & & & & \ddots & \ddots \end{bmatrix}$$

By the definition of edge modes, $\mathbf{u}_j$ must decay to zero as $j \to \infty$ and $j \to -\infty$. Consequently, for sufficiently large j, $|\mathbf{u}_j|$ and $|\mathbf{u}_{-j}|$ become negligibly small. This allows us to impose homogeneous boundary conditions, for some $N \in \mathbb{Z}^+$,

$$\mathbf{u}_{-(N+1)} = \mathbf{0}, \text{ and } \mathbf{u}_{N+1} = \mathbf{0},$$

and truncate (4.19), and consider a finite-dimensional system

$$i\omega \mathbf{v}_N = H_N \mathbf{v}_N \tag{4.20}$$

where

$$\mathbf{v}_N = \begin{bmatrix} \mathbf{u}_{-N} \\ \mathbf{u}_{-(N-1)} \\ \vdots \\ \mathbf{u}_{-1} \\ \mathbf{u}_{1} \\ \vdots \\ \mathbf{u}_{N-1} \\ \mathbf{u}_{N} \end{bmatrix}, \text{ and } H_N = \begin{bmatrix} Q_l & R & & & & & & \\ P & Q_l & R & & & & & \\ & \ddots & \ddots & \ddots & & & & \\ & & P & Q_l & R & & & \\ & & & P & Q & R & & \\ & & & & \ddots & \ddots & \ddots & \\ & & & & & P & Q & R \\ & & & & & & P & Q \end{bmatrix}_{2N\times 2N}.$$

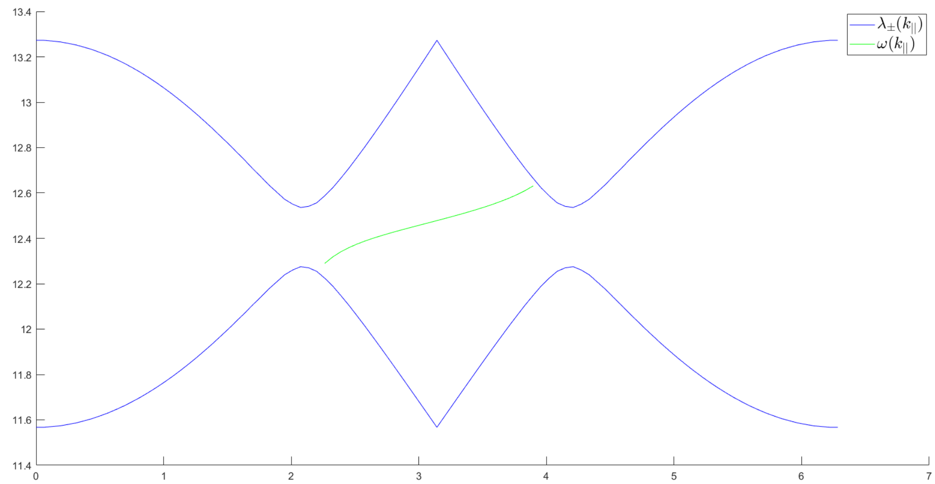

Figure 4.2: The upper and lower bands $\lambda_{\pm}(k_{||})$ and the eigenvalue $\omega(k_{||})$ of H_N in (4.20) when $N = 45$ and $g = 10$.

In Figure 4.2, the graph of the numerical approximation for the edge mode frequency in the band gap is provided. In Figure 4.3, the decaying condition of the edge mode as cells are away from the interface is observed.

4.2.3 An Analysis over Transfer Matrices and Finite System

The transfer matrix approach in Section 4.2.1 is motivated by the decaying property of the edge mode on both sides of the interface. This condition requires the edge mode to be associated with the generalized eigenvector of the transfer matrices whose eigenvalue has modulus less than 1. The interface equations determine whether these decaying solutions match across the interface.

The study on the truncated system in Section 4.2.2 produces some numerical evidence for the existence of edge modes and provides an approximation for the edge mode frequency in the band gap. This approximation should be consistent with the study of transfer matrices. However, when the approximation obtained from the truncated system is applied to the transfer matrices, the calculations fail to satisfy the conditions of the transfer matrix approach.

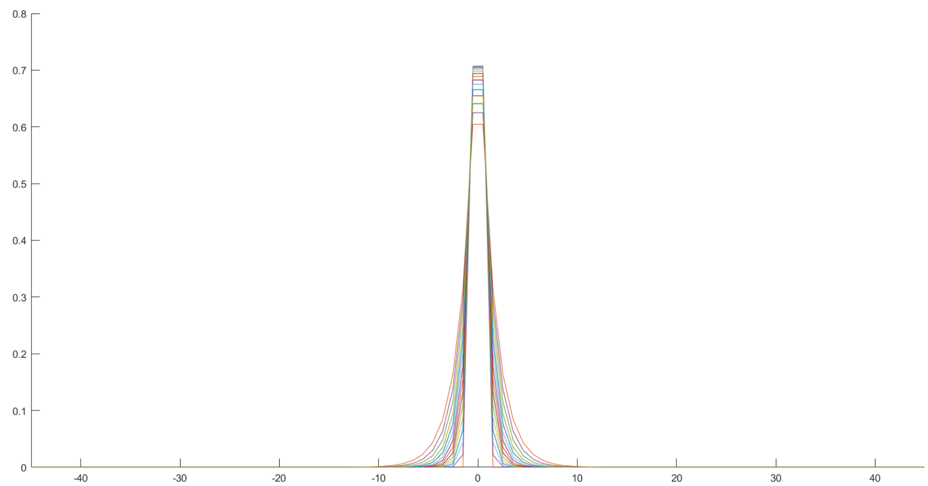

Figure 4.3: The norm of the amplitudes $|u_j| = |\left[x_j^a\, y_j^a\, x_j^b\, y_j^b\right]^t|$ obtained from finite system with edge mode frequency in the band gap. Horizontal axis is the cell indices.

This inconsistency suggests further investigation on the transfer matrix study. One possible source of this discrepancy is the singular transfer matrices. More precisely, singular transfer matrices may affect the associated eigensystem and the edge modes. Another possibility is that the transfer matrix formulation may not fully capture the constraints that are necessary for edge mode calculations.

The precise origin of the discrepancy in the transfer matrix approach and the inconsistency in the transfer matrices and the finite system approximation remains an open question. Nevertheless, Section 4.2.2 provides numerical evidence for the existence of the edge mode and motivates a more detailed analysis Section 4.2.1, transfer matrices.

Chapter 5

Conclusions and Future Work

5.1 Summary

In this dissertation, we studied wave propagation in periodic mechanical topological systems. We developed a mathematical theory for topological phases and the existence of edge modes in such systems.

We analyzed three periodic mechanical systems, their corresponding topological invariants and their interface modes. Depending on the model, the Zak phase, the valley Chern number and the Chern number are the topological invariants studied which characterize the global properties of the bulk spectrum and support the existence of edge modes.

The results emphasize the mathematical challenges associated with one- and two-dimensional models with broken inversion symmetry. In the gyroscopic system where time-reversal symmetry is broken, on the other hand, some additional analytical difficulties appear due to the singularity of the transfer matrices. However, the existence of edge modes is supported by numerical evidence, highlighting problems for further mathematical investigation.

In summary, this dissertation provides a mathematical theory for understanding topological phases and wave localization in periodic mechanical media. By presenting analytical and numerical results, it strengthens the foundation for future studies in different lattices and higher dimensions.

5.2 Open Problems in the Transfer-Matrix Formulation

Despite the effectiveness of the transfer matrix approach in spring-mass systems, several fundamental questions remain open in the gyroscopic setting.

5.2.1 Relation between transfer matrices and truncated systems

A central open problem concerns the relationship between the transfer matrix formulation on infinite domains and numerical results obtained from truncated finite systems. While truncated models show eigenfrequencies in the band gap and the localization of the solution, the precise mathematical connection between these observed modes and the transfer matrix spectrum is not yet fully understood.

5.2.2 Singularity of transfer matrices in gyroscopic systems

In contrast to classical spring-mass systems, transfer matrices arising in gyroscopic lattices are singular. This introduces nontrivial kernels and complicates the propagation of solutions. A deeper understanding of how this degeneracy affects the existence, uniqueness, and stability of edge modes is required. In particular, it is unclear whether additional constraints are necessary to characterize edge states completely.

5.2.3 Numerical approximation and error analysis

Although the numerical simulations on the truncated model exhibit expected qualitative behavior, namely frequency in the band gap and the localization near the interface, a rigorous error analysis is still missing. A quantitative study of convergence rates, finite size effects, and approximation accuracy would provide a more complete justification of the numerical observations.

5.2.4 Toward a rigorous bulk-edge theory

More broadly, a complete mathematical framework for transfer matrices and the existence of edge states in gyroscopic lattices is still lacking. Developing such a theory would clarify the relationship between band structure, topological invariants, and edge modes, thereby strengthening the mathematical foundation of topological mechanical systems.

5.3 Future Directions

5.3.1 Extensions of current models

Several natural extensions of the present work arise from modifications of the geometric and dynamical setting. One direction is the study of interfaces with curved geometry, which would generalize the current interface analysis and introduce new challenges in band structure and edge mode studies.

Another extension concerns one-dimensional systems with boundary conditions involving a fixed point. In such a configuration, one semi-infinite periodic system is coupled to a fixed point boundary which has the trivial topological index, providing a different mechanism for edge states. Higher dimensional analogues include interfaces with embedded defects or constrained boundary directions.

Additionally, damped mechanical systems represent a natural generalization. The presence of damping introduces first order derivatives into the governing equations, leading to richer spectral behavior and potentially new types of localized modes.

5.3.2 Continuous analogues

A second direction concerns continuous models, such as acoustic and elastic media. These systems replace discrete lattice equations with partial differential equations and provide a continuous analogue of the discrete topological systems studied in this work.

Understanding how discrete topological invariants affect continuous settings remains an important open direction.

5.4 Future Directions for Gyroscopic Systems

The present analysis is based on linearized equations of motion. An important extension is the study of nonlinear gyroscopic systems, where amplitude dependent effects may lead to new phenomena such as nonlinear localization, bifurcations of edge states, and energy dependent topological behavior.

Gyroscopic lattices also share structural similarities with chiral phonon systems in solid state physics, where lattice vibrations exhibit intrinsic angular momentum. Investigating this connection may provide further insight into the relationship between topology, energy transport, and wave localization in physical systems.

References

[1] L. D. Landau et al., “On the theory of phase transitions”, Zh. eksp. teor. Fiz **7**, 926 (1937).

[2] K. v. Klitzing, G. Dorda, and M. Pepper, “New method for high-accuracy determination of the fine-structure constant based on quantized hall resistance”, Physical review letters **45**, 494 (1980).

[3] D. J. Thouless, M. Kohmoto, M. P. Nightingale, and M. den Nijs, “Quantized hall conductance in a two-dimensional periodic potential”, Physical review letters **49**, 405 (1982).

[4] M. V. Berry, “Quantal phase factors accompanying adiabatic changes”, Proceedings of the Royal Society of London. A. Mathematical and Physical Sciences **392**, 45–57 (1984).

[5] C. L. Kane and E. J. Mele, “Z 2 topological order and the quantum spin hall effect”, Physical review letters **95**, 146802 (2005).

[6] C. L. Kane and E. J. Mele, “Quantum spin hall effect in graphene”, Physical review letters **95**, 226801 (2005).

[7] B. A. Bernevig, T. L. Hughes, and S.-C. Zhang, “Quantum spin hall effect and topological phase transition in hgte quantum wells”, science **314**, 1757–1761 (2006).

[8] M. Konig, S. Wiedmann, C. Brune, A. Roth, H. Buhmann, L. W. Molenkamp, X.-L. Qi, and S.-C. Zhang, “Quantum spin hall insulator state in hgte quantum wells”, Science **318**, 766–770 (2007).

[9] J. E. Moore, “The birth of topological insulators”, Nature **464**, 194–198 (2010).

[10] F. D. M. Haldane, “Model for a quantum hall effect without landau levels: condensed-matter realization of the” parity anomaly””, Physical review letters **61**, 2015 (1988).

[11] J. E. Moore and L. Balents, “Topological invariants of time-reversal-invariant band structures”, Physical Review B **75**, 121306 (2007).

[12] M. Z. Hasan and C. L. Kane, “Colloquium: topological insulators”, Reviews of modern physics **82**, 3045–3067 (2010).

[13] X.-L. Qi and S.-C. Zhang, “Topological insulators and superconductors”, Reviews of modern physics **83**, 1057–1110 (2011).

[14] F. D. M. Haldane and S. Raghu, “Possible realization of directional optical waveguides in photonic crystals with broken time-reversal symmetry”, Physical review letters **100**, 013904 (2008).

[15] Z. Wang, Y. Chong, J. D. Joannopoulos, and M. Soljačić, “Observation of unidirectional backscattering-immune topological electromagnetic states”, Nature **461**, 772–775 (2009).

[16] A. B. Khanikaev, S. Hossein Mousavi, W.-K. Tse, M. Kargarian, A. H. MacDonald, and G. Shvets, “Photonic topological insulators”, Nature materials **12**, 233–239 (2013).

[17] L. Lu, J. D. Joannopoulos, and M. Soljačić, “Topological photonics”, Nature photonics **8**, 821–829 (2014).

[18] T. Ozawa, H. M. Price, A. Amo, N. Goldman, M. Hafezi, L. Lu, M. C. Rechtsman, D. Schuster, J. Simon, O. Zilberberg, et al., “Topological photonics”, Reviews of Modern Physics **91**, 015006 (2019).

[19] Z. Yang, F. Gao, X. Shi, X. Lin, Z. Gao, Y. Chong, and B. Zhang, “Topological acoustics”, Physical review letters **114**, 114301 (2015).

[20] C. He, X. Ni, H. Ge, X.-C. Sun, Y.-B. Chen, M.-H. Lu, X.-P. Liu, and Y.-F. Chen, "Acoustic topological insulator and robust one-way sound transport", Nature physics **12**, 1124–1129 (2016).

[21] X. Zhang, M. Xiao, Y. Cheng, M.-H. Lu, and J. Christensen, "Topological sound", Communications Physics **1**, 97 (2018).

[22] G. Ma, M. Xiao, and C. T. Chan, "Topological phases in acoustic and mechanical systems", Nature Reviews Physics **1**, 281–294 (2019).

[23] C. L. Kane and T. C. Lubensky, "Topological boundary modes in isostatic lattices", Nature Physics **10**, 39–45 (2014).

[24] B. G.-g. Chen, N. Upadhyaya, and V. Vitelli, "Nonlinear conduction via solitons in a topological mechanical insulator", Proceedings of the National Academy of Sciences **111**, 13004–13009 (2014).

[25] L. M. Nash, D. Kleckner, A. Read, V. Vitelli, A. M. Turner, and W. T. Irvine, "Topological mechanics of gyroscopic metamaterials", Proceedings of the National Academy of Sciences **112**, 14495–14500 (2015).

[26] R. Süsstrunk and S. D. Huber, "Observation of phononic helical edge states in a mechanical topological insulator", Science **349**, 47–50 (2015).

[27] L. Fu and C. Kane, "Superconducting proximity effect and majorana fermions at the surface", in Aps march meeting abstracts (2008), pp. V10–001.

[28] C. Nayak, S. H. Simon, A. Stern, M. Freedman, and S. Das Sarma, "Non-abelian anyons and topological quantum computation", Reviews of Modern Physics **80**, 1083–1159 (2008).

[29] Y. Wu, C. Li, X. Hu, Y. Ao, Y. Zhao, and Q. Gong, "Applications of topological photonics in integrated photonic devices", Advanced Optical Materials **5**, 1700357 (2017).

[30] G.-J. Tang, X.-T. He, F.-L. Shi, J.-W. Liu, X.-D. Chen, and J.-W. Dong, "Topological photonic crystals: physics, designs, and applications", Laser & photonics reviews **16**, 2100300 (2022).

[31] R. Chaunsali, F. Li, and J. Yang, "Stress wave isolation by purely mechanical topological phononic crystals", Scientific reports **6**, 30662 (2016).

[32] D. J. Apigo, W. Cheng, K. F. Dobiszewski, E. Prodan, and C. Prodan, "Observation of topological edge modes in a quasiperiodic acoustic waveguide", Physical review letters **122**, 095501 (2019).

[33] C. Fefferman and M. Weinstein, "Honeycomb lattice potentials and dirac points", Journal of the American Mathematical Society **25**, 1169–1220 (2012).

[34] C. L. Fefferman and M. I. Weinstein, "Wave packets in honeycomb structures and two-dimensional dirac equations", Communications in Mathematical Physics **326**, 251–286 (2014).

[35] C. L. Fefferman, J. P. Lee-Thorp, and M. I. Weinstein, "Edge states in honeycomb structures", Annals of PDE **2**, 1–80 (2016).

[36] C. Fefferman, J. Lee-Thorp, and M. Weinstein, *Topologically protected states in one-dimensional systems*, Vol. 247, 1173 (American Mathematical Society, 2017).

[37] J. P. Lee-Thorp, M. I. Weinstein, and Y. Zhu, "Elliptic operators with honeycomb symmetry: dirac points, edge states and applications to photonic graphene", Archive for Rational Mechanics and Analysis **232**, 1–63 (2019).

[38] A. Drouot, "Characterization of edge states in perturbed honeycomb structures", Pure and Applied Analysis **1**, 385–445 (2019).

[39] J. Lin and H. Zhang, "Mathematical theory for topological photonic materials in one dimension", Journal of Physics A: Mathematical and Theoretical **55**, 495203 (2022).

[40] J. Qiu, J. Lin, P. Xie, and H. Zhang, “Mathematical theory for the interface mode in a waveguide bifurcated from a dirac point”, arXiv preprint arXiv:2304.10843 (2023).

[41] A. Drouot and M. I. Weinstein, “Edge states and the valley hall effect”, Advances in Mathematics **368**, 107142 (2020).

[42] A. Drouot, C. L. Fefferman, and M. I. Weinstein, “Defect modes for dislocated periodic media”, Communications in Mathematical Physics **377**, 1637–1680 (2020).

[43] Y. Hatsugai, “Chern number and edge states in the integer quantum hall effect”, Physical review letters **71**, 3697 (1993).

[44] H. Schulz-Baldes, J. Kellendonk, and T. Richter, “Simultaneous quantization of edge and bulk hall conductivity”, Journal of Physics A: Mathematical and General **33**, L27–L32 (2000).

[45] P. Elbau and G.-M. Graf, “Equality of bulk and edge hall conductance revisited”, Communications in mathematical physics **229**, 415–432 (2002).

[46] A. Elgart, G. Graf, and J. Schenker, “Equality of the bulk and edge hall conductances in a mobility gap”, Communications in mathematical physics **259**, 185–221 (2005).

[47] G. Bal, “Topological invariants for interface modes”, Communications in Partial Differential Equations **47**, 1636–1679 (2022).

[48] G. Bal, “Topological protection of perturbed edge states”, arXiv preprint arXiv:1709.00605 (2017).

[49] G. Bal, “Continuous bulk and interface description of topological insulators”, Journal of Mathematical Physics **60** (2019).

[50] A. B. Khanikaev, R. Fleury, S. H. Mousavi, and A. Alu, “Topologically robust sound propagation in an angular-momentum-biased graphene-like resonator lattice”, Nature communications **6**, 8260 (2015).

[51] J. Lu, C. Qiu, M. Ke, and Z. Liu, “Valley vortex states in sonic crystals”, Physical review letters **116**, 093901 (2016).

[52] L. Ye, C. Qiu, J. Lu, X. Wen, Y. Shen, M. Ke, F. Zhang, and Z. Liu, “Observation of acoustic valley vortex states and valley-chirality locked beam splitting”, Physical Review B **95**, 174106 (2017).

[53] T. Ma and G. Shvets, “All-si valley-hall photonic topological insulator”, New Journal of Physics **18**, 025012 (2016).

[54] L.-H. Wu and X. Hu, “Scheme for achieving a topological photonic crystal by using dielectric material”, Physical review letters **114**, 223901 (2015).

[55] R. K. Pal, J. Vila, and M. Ruzzene, “Topologically protected edge states in mechanical metamaterials”, Advances in Applied Mechanics **52**, 147–181 (2019).

[56] X. Zheng, J. Zhao, N. Kacem, and P. Liu, “Toward acceleration sensing based on topological gyroscopic metamaterials”, Physical Review B **106**, 094307 (2022).

[57] D. Vanderbilt, *Berry phases in electronic structure theory: electric polarization, orbital magnetization and topological insulators* (Cambridge University Press, 2018).

[58] J. Lin and H. Zhang, “Mathematical theory for topological photonic materials in one dimension”, Journal of Physics A: Mathematical and Theoretical **55**, 495203 (2022).

[59] C. L. Fefferman, J. P. Lee-Thorp, and M. I. Weinstein, “Honeycomb schrödinger operators in the strong binding regime”, Communications on Pure and Applied Mathematics **71**, 1178–1270 (2018).

[60] D. Xiao, W. Yao, and Q. Niu, “Valley-contrasting physics in graphene: magnetic moment and topological transport”, Physical review letters **99**, 236809 (2007).

[61] D. Xiao, M.-C. Chang, and Q. Niu, “Berry phase effects on electronic properties”, Reviews of modern physics **82**, 1959 (2010).

[62] R. Resta and D. Vanderbilt, "Theory of polarization: a modern approach", in *Physics of ferroelectrics: a modern perspective* (Springer, 2007), pp. 31–68.

Appendix A

Supplementary Figures for Chapter 2

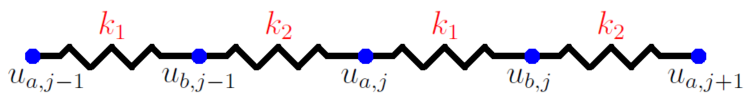

Figure A.1: One-dimensional lattice consisting of an array of masses connected by springs.

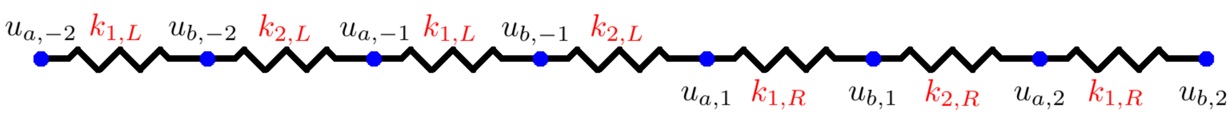

Figure A.2: The topological mechanical system in one dimension

Appendix B

Supplementary Figures for Chapter 3

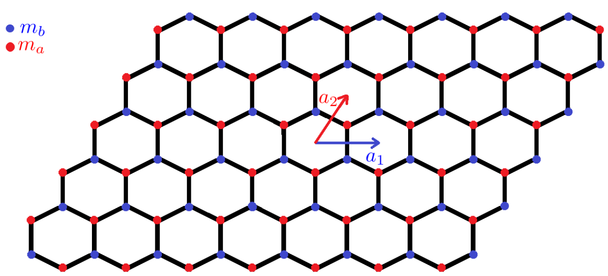

(a) The periodic mechanical system.

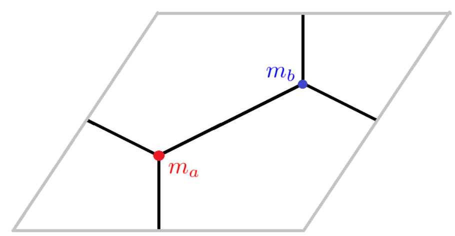

(b) Periodic cell $Y_{p,q} = \{(p + t_1)\mathbf{a_1} + (q + t_2)\mathbf{a_2} : 0 \leq t_1, t_2 \leq 1\}$.

Figure B.1: The periodic mechanical system over the honeycomb lattice.

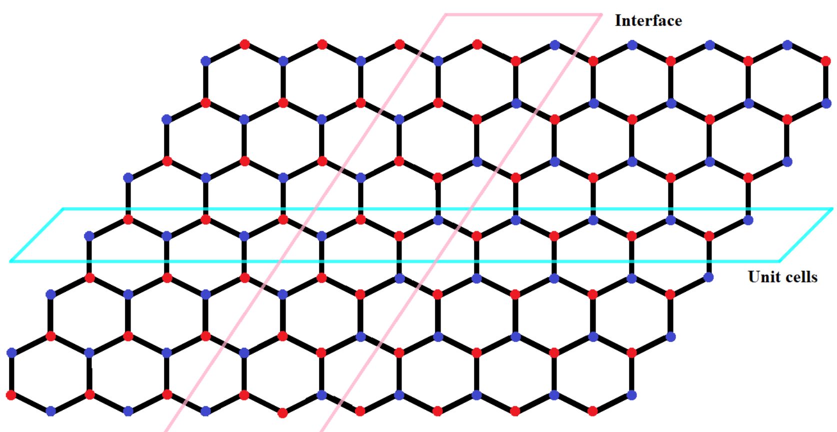

Figure B.2: The topological mechanical system formed by two hexagonal lattices with opposite β values. The interface direction is parallel to $\mathbf{a}_2$.

Appendix C

Supplementary Figures for Chapter 4

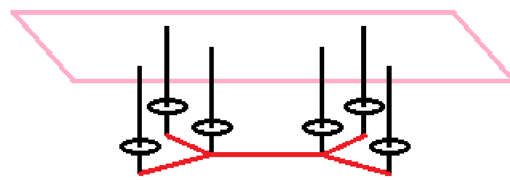

Figure C.1: Gyroscopic mechanical system. Gyroscopes are hanged to a plate and their tips are joined each other by identical springs and form hexagonal lattice.

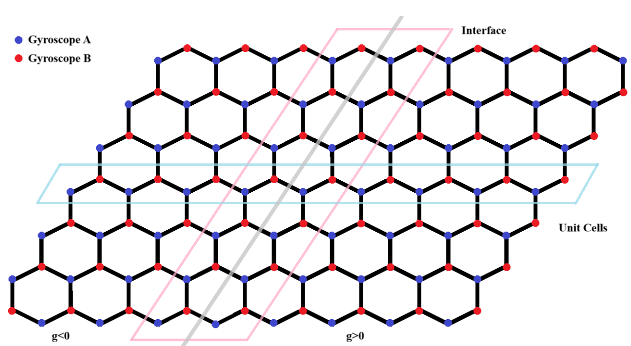

Figure C.2: The gyroscopic mechanical system formed by two hexagonal lattice with opposite sign g. The interface is parallel to $\mathbf{a}_2$ direction.